Article

Cancer Cell

miR-126 Regulates Distinct Self-Renewal Outcomes in Normal and Malignant Hematopoietic Stem Cells

Graphical Abstract

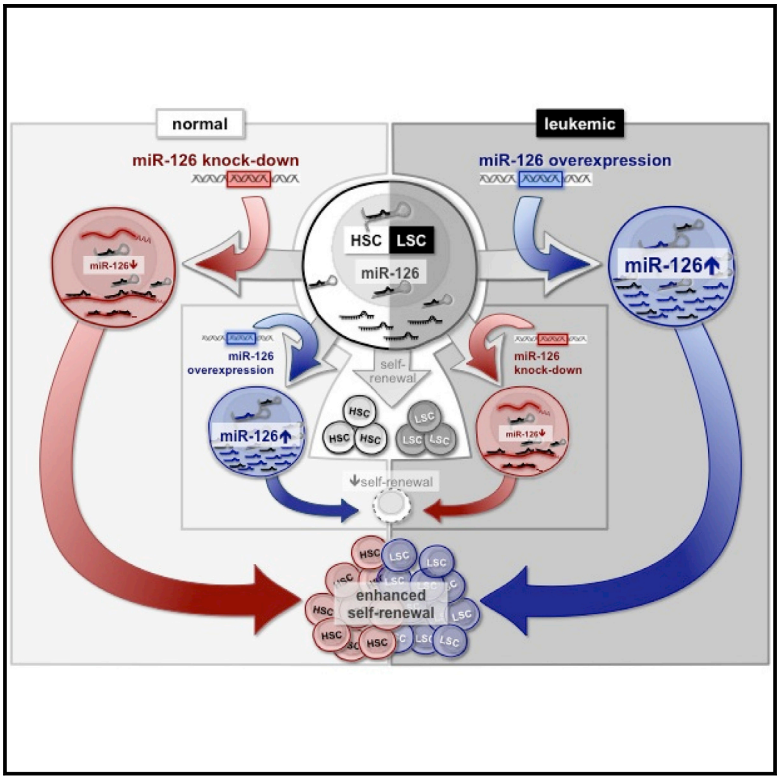

Authors

Eric R. Lechman, Bernhard Gentner, Stanley W.K. Ng, ..., Jean C.Y. Wang, Luigi Naldini, John E. Dick

Correspondence

jdick@uhnresearch.ca

In Brief

Lechman et al. show that miR-126 targets the PI3K/AKT/MTOR signaling pathway to preserve quiescence, increase self-renewal, and promote chemotherapy resistance of acute myeloid leukemia stem cells (LSC). Reducing the miR-126 level impairs LSC maintenance in contrast to expanding normal hematopoietic stem cells.

Highlights

- Clinical outcome in AML correlates with LSC-associated miRNA expression
- miR-126 targets multiple components of the PI3K/AKT/MTOR signaling pathway
- miR-126 promotes chemotherapy resistance by preserving LSC in a quiescent state
- miR-126 governs opposing self-renewal outcomes in normal and malignant stem cells

Accession Numbers

GSE55917
GSE55814
GSE55770
PXD001994

Lechman et al., 2016, Cancer Cell *29*, 214–228
February 8, 2016
http://dx.doi.org/10.1016/j.ccell.2015.12.011

CellPress

CellPress

Cancer Cell
Article

miR-126 Regulates Distinct Self-Renewal Outcomes in Normal and Malignant Hematopoietic Stem Cells

Eric R. Lechman,[1,2,16] Bernhard Gentner,[3,4,5,16] Stanley W.K. Ng,[6,7] Erwin M. Schoof,[1,2] Peter van Galen,[1,2] James A. Kennedy,[1,8] Silvia Nucera,[3,4] Fabio Ciceri,[4,5] Kerstin B. Kaufmann,[1,2] Naoya Takayama,[1,2] Stephanie M. Dobson,[1,2] Aaron Trotman-Grant,[1,2] Gabriela Krivdova,[1,2] Janneke Elzinga,[1,2] Amanda Mitchell,[1,2] Björn Nilsson,[9] Karin G. Hermans,[1,2] Kolja Eppert,[10] Rene Marke,[11] Ruth Isserlin,[7] Veronique Voisin,[7] Gary D. Bader,[7] Peter W. Zandstra,[6,7] Todd R. Golub,[12] Benjamin L. Ebert,[13] Jun Lu,[14] Mark Minden,[1,8] Jean C.Y. Wang,[1,8] Luigi Naldini,[3,4] and John E. Dick[1,2,15,*]

[1]Princess Margaret Cancer Centre, University Health Network
[2]Department of Molecular Genetics
University of Toronto, Toronto, ON M5G 1L7, Canada
[3]San Raffaele Telethon Institute for Gene Therapy
[4]Vita Salute San Raffaele University, San Raffaele Scientific Institute
[5]Hematology and Bone Marrow Transplantation Unit
San Raffaele Hospital, Milan 20132, Italy
[6]Department of Chemical Engineering and Applied Chemistry, Institute of Biomaterials and Biomedical Engineering, University of Toronto, Toronto, ON M5G 2M9, Canada
[7]The Donnelly Centre, University of Toronto, Toronto, ON M5S 3E1, Canada
[8]Department of Medicine, University of Toronto, Toronto, ON M5G 2M9, Canada
[9]Department of Hematology and Transfusion Medicine, Lund University Hospital, Lund 221 84, Sweden
[10]Department of Pediatrics, McGill University and The Research Institute of the McGill University Health Centre, Montreal, QC H4A 3J1, Canada
[11]Laboratory of Pediatric Oncology, Radboud University Medical Center, Nijmegen, 6500 HB, Netherlands
[12]Department of Pediatric Oncology, Dana-Farber Cancer Institute, 44 Binney Street, Boston, MA 02115, USA
[13]Division of Hematology, Department of Medicine, Brigham and Women's Hospital, Harvard Medical School, Boston, MA 02115, USA
[14]Yale Stem Cell Center, Yale Cancer Center, Yale University School of Medicine, New Haven, CT 06520, USA
[15]Princess Margaret Cancer Research Tower, Room 8-301, 101 College Street, Toronto M5G 1L7, Canada
[16]Co-first author
*Correspondence: jdick@uhnresearch.ca
http://dx.doi.org/10.1016/j.ccell.2015.12.011

SUMMARY

To investigate miRNA function in human acute myeloid leukemia (AML) stem cells (LSC), we generated a prognostic LSC-associated miRNA signature derived from functionally validated subpopulations of AML samples. For one signature miRNA, miR-126, high bioactivity aggregated all in vivo patient sample LSC activity into a single sorted population, tightly coupling miR-126 expression to LSC function. Through functional studies, miR-126 was found to restrain cell cycle progression, prevent differentiation, and increase self-renewal of primary LSC in vivo. Compared with prior results showing miR-126 regulation of normal hematopoietic stem cell (HSC) cycling, these functional stem effects are opposite between LSC and HSC. Combined transcriptome and proteome analysis demonstrates that miR-126 targets the PI3K/AKT/MTOR signaling pathway, preserving LSC quiescence and promoting chemotherapy resistance.

Significance

Leukemia stem cells play central roles in disease progression and recurrence due to their intrinsic capacity for self-renewal and chemotherapy resistance. However, few regulators of human LSC function are known. Our study establishes that miRNA plays a powerful role in governing the fundamental properties that define the stemness state of human LSC including quiescence, self-renewal, and chemotherapy response. Self-renewal regulators have remarkably parallel functions in malignant and normal stem cells, precluding their therapeutic targeting because of toxicity to normal stem cells. The opposing self-renewal outcomes governed by miR-126 within HSC and LSC indicate that despite shared stemness determinants, it may be possible to target therapeutically the networks that specifically control LSC through perturbation of miR-126 levels.

INTRODUCTION

Acute myeloid leukemia (AML) is organized as an aberrant developmental hierarchy maintained by functionally distinct leukemia stem cells (LSC) (Kreso and Dick, 2014). LSC are linked to therapy failure and disease recurrence, but they also share many biological properties with hematopoietic stem cells (HSC), including capacity for self-renewal and quiescence (Kreso and Dick, 2014). Several self-renewal regulators have been studied in both HSC and LSC contexts including PTEN, BMI1, GFI1, TEL1, STAT5, and JUNB; except for PTEN, loss of function typically impairs self-renewal of both LSC and HSC (Yilmaz and Morrison, 2008). LSC and HSC are both quiescent, although quiescence regulation is better understood in HSC. Several intrinsic and extrinsic signals converge upon cyclins and cyclin-dependent kinases (CDKs) that act upstream of Retinoblastoma (RB) family members to regulate early and late G_1 progression in HSC (Viatour et al., 2008), while the G_0 state is governed by MTORC1 and CDK6 (Laurenti et al., 2015; Rodgers et al., 2014). Quiescence and distinct G_0 exit kinetics are essential HSC properties (Trumpp et al., 2010). Although LSC quiescence is less well defined, the known regulators appear to function similarly in LSC and HSC, with LSC quiescence often invoked as a mechanism of chemotherapy resistance (Holtz et al., 2007). Additional studies are required to determine if differences exist in self-renewal and quiescence regulation between LSC and HSC and whether it is possible to develop therapies that eradicate LSC while sparing HSC.

Transcriptional analysis of human HSC and functionally defined LSC have defined stemness signatures that are highly prognostic for patient survival, establishing that LSC-specific properties are clinically relevant (Eppert et al., 2011; Metzeler et al., 2013). However, little is known of how stemness programs are controlled. Several differentially expressed miRNAs were identified and found to control HSC (Hu et al., 2015; Lechman et al., 2012; Mehta et al., 2015; O'Connell et al., 2010) by coordinate repression of multiple targets (Ebert and Sharp, 2012). In hematopoiesis, most miRNAs affect progenitor lineage commitment and mature cell function (Undi et al., 2013), although HSC self-renewal can be governed by miR-125a/b, miR-29a, and miR-126 (Ooi et al., 2010; O'Connell et al., 2010; Guo et al., 2010; Lechman et al., 2012). miR-126 plays a role, conserved in both human and mouse, in maintaining HSC quiescence by attenuating the cellular response to extrinsic signals via targeting multiple components of the PI3K/AKT/GSK3B signaling pathway (Lechman et al., 2012). Thus, HSC expand without concomitant exhaustion upon miR-126 silencing.

Deregulation of miRNAs occurs in leukemia correlating with known risk categories and prognosis (Garzon et al., 2008; Li et al., 2008; Marcucci et al., 2009). Functionally, miRNA overexpression can induce murine leukemic transformation (Han et al., 2010; O'Connell et al., 2010; Song et al., 2013). Several LSC-associated miRNAs are functional: miR-17-92 polycistron maintained LSC in MLL models (Wong et al., 2010), whereas antagonizing miR-196 and miR-21 reduced LSC in an experimental human MLL model (Velu et al., 2014). Targeted miR-126 reduction in cell lines and primary AML samples reduced AML growth, although mechanisms were not reported (Dorrance et al., 2015; de Leeuw et al., 2014). These promising studies point to the importance of further understanding the role of miRNA in governing stemness in AML. Here, we investigated the role of miR-126 in governing LSC self-renewal, quiescence, and chemotherapy resistance.

RESULTS

LSC miRNA Signature Is Prognostic for Patient Outcome

To determine whether miRNA are differentially expressed in LSC and HSC, we fractionated 16 AML patient samples and three lineage-depleted (Lin^-) cord blood (CB) samples using CD34 and CD38 into four populations and subjected each to global miRNA profiling; the stem cell content of each fraction was functionally assayed by xenotransplantation (Figures 1A and S1A). Bioinformatic analysis of 25 LSC-enriched and 27 fractions devoid of LSC activity (Figure S1A) revealed a human LSC-associated miRNA signature derived from in vivo functionally validated AML patient samples (Figure 1B). In parallel, miRNAs enriched in HSC or committed progenitors were determined (Figure S1B). By comparing similar immunophenotypic AML and normal populations, several differentially expressed miRNAs were found (Figure S1C).

To determine if the LSC-associated miRNA signature was clinically relevant, a regression analysis was performed on 74 AML patients with normal cytogenetics (PMCC cohort, Table S1). An optimized LSC signature consisting of four miRNAs was identified, each with differential weights based on impact upon overall survival (OS) (Figure 1C). This signature was prognostic of OS in both univariate (Figure 1D) and multivariate analyses (Figure 1E) in an independent cohort. Together with prior studies showing that LSC-specific gene expression signatures are significantly prognostic (Eppert et al., 2011; Greaves, 2011), these data establish that LSC properties influence clinical outcomes and that miRNAs play a powerful role in regulating LSC stemness.

miR-126 Bioactivity Enriches for LSC Activity

Further functional studies on AML focused on miR-126 as it is a known HSC regulator (Lechman et al., 2012). qPCR independently confirmed that LSC-containing AML fractions generally expressed the highest miR-126 levels (Figure S2A). As miRNA expression does not uniformly equate with miRNA bioactivity, a miR-126 lentiviral reporter vector was used to investigate whether miR-126 is biologically active in LSC (Gentner et al., 2010); ΔNGFR levels indicate transduced cells, while EGFP levels are inversely correlated with miR-126 bioactivity (Figure S2B). Four primary AML samples (Table S2) were transduced with the reporter, transplanted into xenografts, and after 12 weeks the engrafting population was sorted solely on the basis of miR-126 bioactivity (Figure 2A). Each sorted population was transplanted into secondary mice and LSC activity scored after 8 weeks, based on whether the engrafting population recapitulated the same EGFP/ΔNGFR flow profile as the primary recipient (a cardinal property of cancer stem cells). Despite the presence of LSC activity in multiple subpopulations with CD34 and CD38 sorting (Table S2), miR-126 bioactivity aggregated all LSC activity into a single $miR\text{-}126^{high}$ population (Figure 2B). qPCR confirmed 40-fold higher mature miR-126 levels in LSC-engrafting fractions compared with non-engrafting fractions for three AML samples (Figure S2C). LSC-containing fractions also had the highest clonogenic (Figure S2D) and proliferative

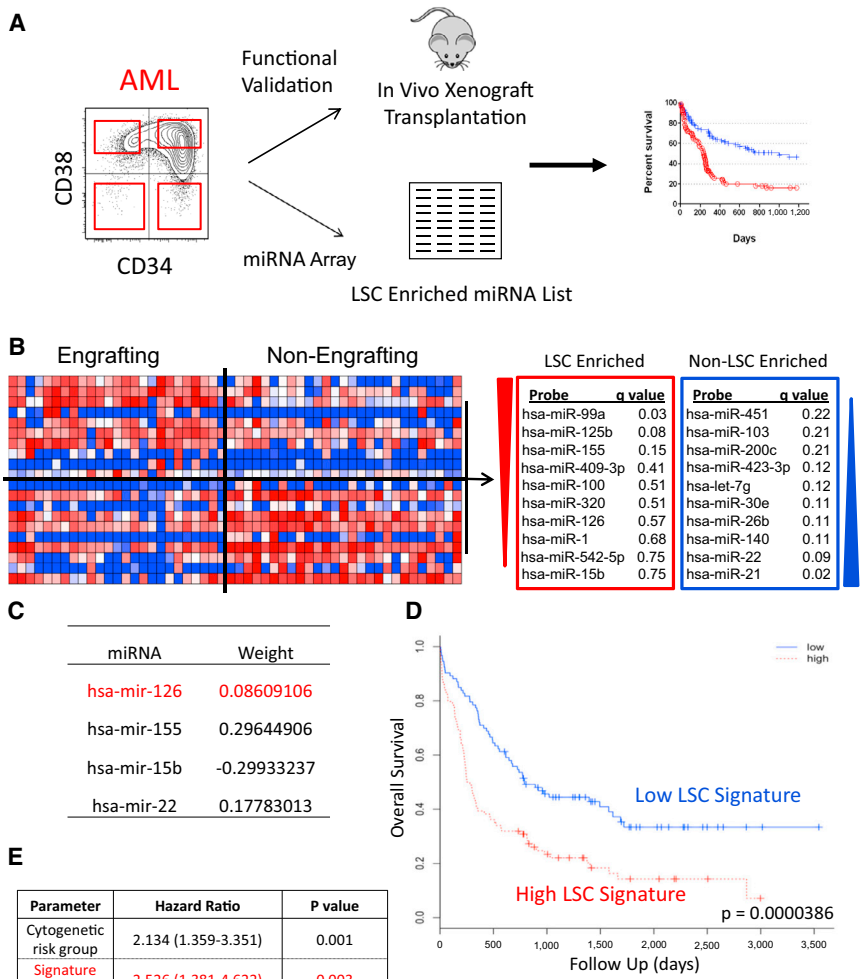

Figure 1. Generation and Validation of an LSC-Enriched miRNA Signature

(A) Schematic depicting the strategy to fractionate human AML patient samples based on immunophenotypic staining for CD34 and CD38. Functional validation of sorted fractions was performed by xenotransplantation, the result of which was combined with miRNA expression profiling to generate stem cell-related miRNA expression profiles.

(B) Heatmap and summary of miRNAs enriched within the LSC and non-LSC populations.

(C) The optimized miRNA signature derived from regression analysis of the PMCC cohort and the weight each miRNA adds to the overall signature.

(D and E) Validation of the optimized LSC-associated miRNA signature shown in (C) in the TCGA cohort (n = 187) by (D) univariate analysis (hazard ratio [HR], 2.04; $p < 0.0001$) and (E) multivariate analysis (HR, 2.53; $p = 0.003$). See also Figure S1 and Table S1.

potential (Figure S2E). These data indicate that miR-126 bioactivity is directly linked to LSC function and that it is possible to exploit miRNA bioactivity for prospective LSC isolation, circumventing often unreliable and heterogeneously expressed cell surface markers (Kreso and Dick, 2014).

Clinical Relevance of miR-126 Expression

To determine if miR-126 expression alone is prognostic, the PMCC cohort (Table S1) was investigated, and increased miR-126 expression was found to be associated with worse OS (median OS of 28.5 months [high expression] versus not reached [low expression]; Figure 2C), event-free survival (Figure 2D), and relapse-free survival (Figure 2E), a result in keeping with other studies (Dorrance et al., 2015; de Leeuw et al., 2014). Since miR-126 expression is high in patients with t(8; 21) and inv(16) (Li et al., 2008), we evaluated the prognostic value of miR-126 after excluding these patients from The Cancer Genome Atlas (TCGA) dataset. High miR-126 was associated with decreased survival in the TCGA dataset (median OS of 12.3 months [high expression] versus 18.5 months [low expression]; Figure 2F). The prognostic significance of miR-126 further strengthens the link between AML patient outcomes, stemness properties, and the regulatory of role of miRNA (Greaves, 2011).

Development of a Functionally Relevant Human AML Model for Mechanistic Studies

How miR-126 functions throughout the AML hierarchy is difficult to investigate since functional studies in primary AML cells are technically challenging and hitherto no human AML cell lines recapitulate the hierarchical organization of primary cells. Therefore, we developed an indefinitely growing AML culture system (8227) from a relapse sample that is organized as a functional hierarchy (Figure 3A) (E.L., unpublished data). Expression of CD34 and CD38 is tightly linked to the functional hierarchy; $CD34^+CD38^-$ cells possess LSC activity and contain a quiescent population, by contrast $CD34^+CD38^+$ cells are enriched in clonogenic progenitors and the remaining 90% of $CD34^-CD38^+$ and $CD34^-CD38^-$ cells are terminally differentiated $CD15^+CD14^+$ blasts (Figure 3A). We show through an integrated analysis of function, phenotype, miR-126 bioactivity, and promoter methylation status on all sorted fractions that high miR-126 levels correlate with the $CD34^+CD38^-$ phenotype and LSC activity and are linked to EGFL7 expression and stem cell-specific promoter methylation patterns (Figure S3A and E.L., unpublished data). Thus, 8227 cells are a relevant model culture system for interrogating the functional effects of miR-126 activity within the context of a leukemic hierarchy.

miR-126 Expression Induces Quiescence in Primitive AML Cells

To investigate the functional importance of miR-126 within the AML developmental hierarchy, 8227 cells were transduced

A

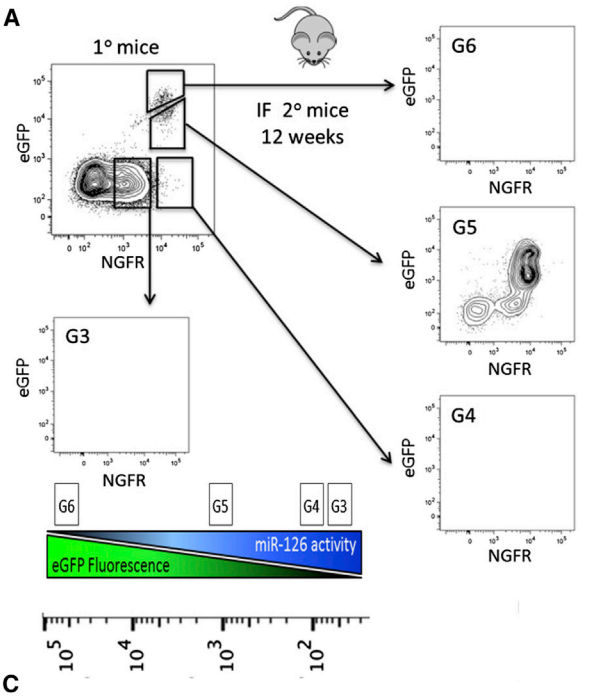

B

AML	Population Gate	Cell # injected per mouse	$CD45^+/NGFR^+/eGFP^+$ Engraftment	miR-126 Reporter Status
AML 1	G6	20,000	0/4 mice	Low
	G5	20,000	0/4 mice	High
	G4/G3	20,000	4/4 mice	High
AML 3	G6	6,050	0/4 mice	Low
	G5	8,500	1/4 mice	High
	G4	1,466	0/4 mice	High
	G3	100,000	0/4 mice	High
AML 7	G6	88,000	0/5 mice	Low
	G5	88,000	0/5 mice	High
	G4	50,000	0/5 mice	High
	G3	40,000	5/5 mice	High
AML 18	G6	2,100	0/4 mice	Low
	G5	18,250	3/3 mice	High
	G4	22,500	0/4 mice	High
	G3	70,500	0/4 mice	High

C

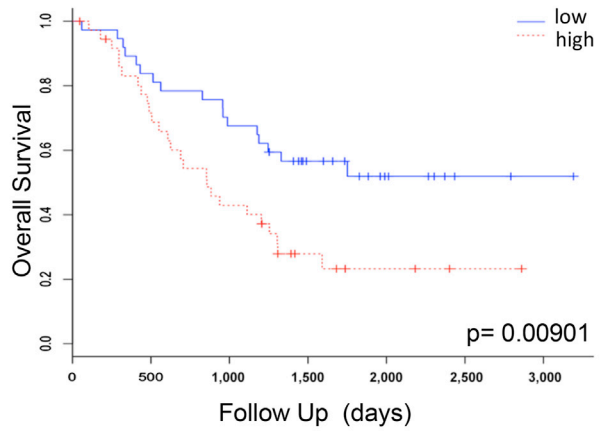

D

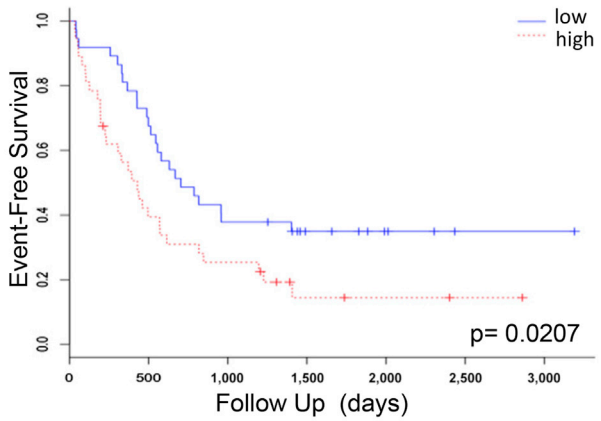

E

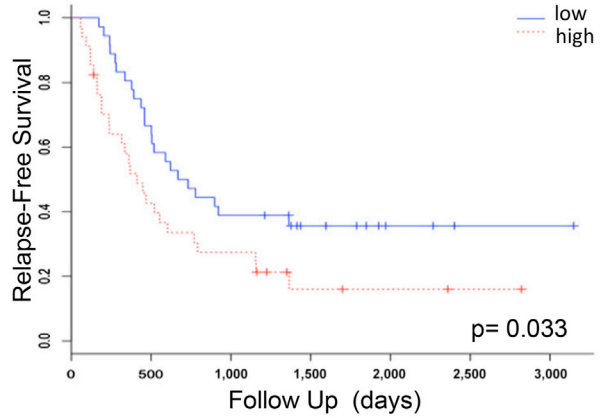

F

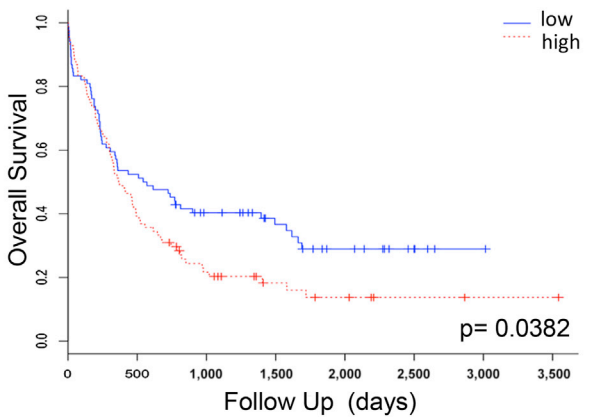

(legend on next page)

with an mOrange (mO) lentivirus expressing miR-126 (126OE) or empty control vector (CTRL) (Figure S3B), and elevated miR-126 levels were confirmed (Figure 3B). Following in vitro propagation of transduced cells, the $mO^+CD34^+CD38^-$ (surrogate LSC) population was sorted and the proliferative, differentiation, and clonogenic capacity was evaluated over 28 days. By 7 days, primitive $CD34^+$ cells increased (Figure 3C) and differentiated $CD14^+CD15^+$ cells decreased (Figure S3C) in the 126OE group. This proportional increase in $CD34^+$ cells correlated to transient reductions in clonogenicity of day 0 bulk cultures (Figure S3D); a reduction primarily confined to $CD34^+CD38^+$ clonogenic fractions (Figure 3D). Bulk cultures of the 126OE group had significantly decreased (15%) bromodeoxyuridine (BrdU) incorporation at 3 hr ($p = 0.002$) and 16 hr ($p = 0.001$) compared with CTRL (Figure 3E). No differences in apoptosis were observed (data not shown). Cell cycle analysis of sorted 126OE populations at 7 days showed 2-fold increased proportions of quiescent (G_0) $CD34^+CD38^-$ cells and decreased $S/G_2/M$ cells (Figures 3F and S3E). By contrast, the G_0 status of 126OE $CD34^+CD38^+$ and $CD34^-$ populations remained unaffected (data not shown). Thus, 126OE maintains 8227 cells in a more primitive state by increasing the proportion of quiescent $CD34^+CD38^-$ cells, thereby decreasing the overall proliferative output and differentiation of AML blasts.

miR-126 Knockdown Provokes LSC Entry into Cycle

To determine the impact of miR-126 knockdown, 8227 cells were transduced with lentiviruses that were empty (CTRL) or expressing an miR-126 sponge (126KD) (Figure S3F) (Lechman et al., 2012). Following sorting and culture, 126KD of the $EGFP^+$ $CD34^+CD38^-$ population resulted in increased output of $CD34^+$ cells at all time points (Figure 3G), without increasing differentiation (Figure S3G). This effect was primarily localized to the $CD34^+CD38^-$ compartment (Figure 3H). Clonogenic potential within the $CD34^+CD38^-$ LSC-enriched compartment increased while no differences were observed in the $CD34^+CD38^+$ progenitor-enriched compartment (Figure 3I). 126KD increased BrdU incorporation by 20% at 3 hr ($p = 0.0024$) and 16 hr ($p = 0.0093$) (Figure 3J) without affecting apoptosis (data not shown). Upon 126KD, the proportion of cells in G_0 was decreased (30%) and $S/G_2/M$ increased (3-fold) within $EGFP^+CD34^+CD38^-$ populations (Figures 3K and S3H). 126KD of $CD34^+CD38^+$ cells trended in the same direction (CTRL G_0 16.07% versus 126KD G_0 11.54%, $p = 0.2$); $CD34^-$ and non-transduced populations were unaffected (data not shown). Within bulk 126KD cultures, the increased cell cycle and clonogenicity (Figure S3I) was primarily due to effects on $CD34^+CD38^-$ cells (Figure 3H). As LSC-enriched $CD34^+CD38^-$ cells are less clonogenic than $CD34^+CD38^+$ cells, we interpret these data as 126KD driving $CD34^+CD38^-$ cells out of their quiescent stem-like state and into a more committed population of proliferating clonogenic cells while retaining a primitive cell surface phenotype.

Enforced Expression of miR-126 Expands LSC In Vivo

To test the prediction that miR-126 maintains a primitive state by restraining entry into the cell cycle of LSC from patients, nine AML samples were transduced with 126OE and CTRL vectors and transplanted into NSG mice (Tables S2 and S3). Transduction efficiency and expression varied (Figures S4A and S4B), while leukemic engraftment was similar between CTRL and 126OE groups (Figure S4C). Although the initial transduction efficiency was ~50% lower for 126OE than CTRL in six of nine AML samples, $mOrange^+$ cells within the human $CD45^+$ graft was higher for six of nine AML samples indicating a competitive advantage for 126OE groups (Figure S4D). Analysis of primitive cell engraftment used both CD34 and CD117, as CD117 is associated with AML clinical outcome and correlated with miR-126 expression (de Leeuw et al., 2014; Schneider et al., 2015). Phenotypic primitive cells were increased in 126OE groups for seven of nine samples (Figure 4A) with concomitant reduction of differentiated cells; four of nine samples showed a significant reduction for $CD15^+$ cells (Figure 4B), and six of nine showed a trend for reduced $CD14^+$ blasts (Figure S4E). 126OE caused an increase in $CD15^+$ blasts for two samples (Figure 4B).

To evaluate 126OE on LSC function within the xenografts, serial transplantation with limiting dilution analysis was used to quantify LSC numbers. In three samples, LSC frequency increased in the 126OE group (Figures 4C and S4F). Although individual patient samples exhibited variation, overall, 126OE increased LSC self-renewal and reduced differentiation leading to LSC expansion.

miR-126 Knockdown Targets LSC In Vivo

126KD was used to determine whether reducing miR-126 would impair AML engraftment or LSC function (Figure S5A). Total levels of human $CD45^+$ (Figure S5B) or $CD45^+EGFP^+$ engraftment (Figure S5C) were unaffected in the 126KD group, although there was heterogeneity. By contrast, primitive $CD117^+$ blasts were reduced in three of seven in the 126KD group, while two of seven had increased $CD117^+$ blasts (Figure 5A); differentiated $CD15^+CD14^+$ cells were increased in four of seven samples (Figure 5B). The LSC frequency was reduced in two of three samples

Figure 2. miR-126 Bioactivity Marks the Functional LSC Compartment in Human AML

(A) Schematic describing the sorting scheme/scoring system for secondary mice. AML samples were transduced with an miR-126 reporter construct and transplanted into conditioned NSG mice for 12 weeks. Bone marrow was analyzed for engraftment using $CD45^+\Delta NGFR^+EGFP^+$ staining. Cells were sorted into four populations based on ΔNGFR (transduced cells) and EGFP expression (inverse of miR-126 bioactivity), counted, and injected into secondary mice for 8–10 weeks. When a ΔNGFR/EGFP profile is recapitulated in secondary mice, the mouse is scored as engrafted.

(B) Summary of the results of the miR-126 bio-reporter assays.

(C) Kaplan-Meier overall survival (OS) curves in the PMCC CN AML cohort (n = 74) according to the miR-126 expression level (HR, 2.23; p = 0.00901).

(D) Univariate Cox model analysis for miR-126 as prognostic for event-free survival in the PMCC cohort of CN AML patients (n = 74; p = 0.0207, log rank test, median split; HR, 1.8744; p = 0.0207, Wald test).

(E) Kaplan-Meier survival curves correlating miR-126 expression and relapse-free survival in the PMCC patient cohort. Univariate median split log rank test (HR, 1.7995; p = 0.033, Wald test).

(F) Univariate analysis for OS in the TGCA AML cohort that encompasses all levels of cytogenetic risk (n = 187) according to the miR-126 expression level (HR, 1.41; p = 0.0382). See also Figure S2.

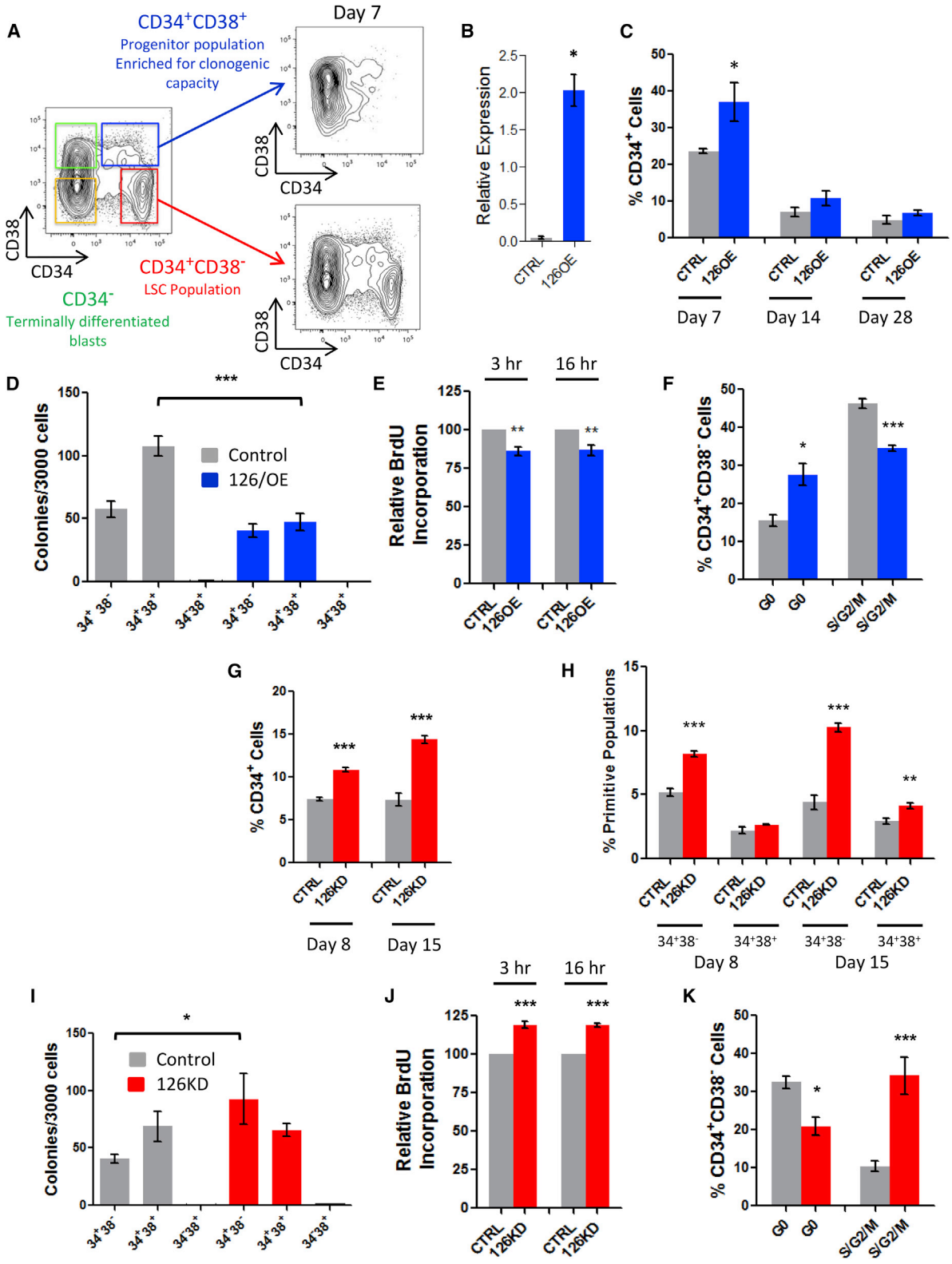

Figure 3. Enforced Expression and Knockdown of miR-126 Alters the Proliferation and Differentiation Status of Primitive 8227 AML Cells

(A) Illustration showing flow plots of CD34 and CD38 immunostained 8227 cultures. The red gated ($CD34^+CD38^-$) population is enriched in quiescent LSC and reinitiates the original hierarchy in vitro after flow sorting. The blue gated population ($CD34^+CD38^+$) is enriched in colony-forming unit (CFU) potential and

(legend continued on next page)

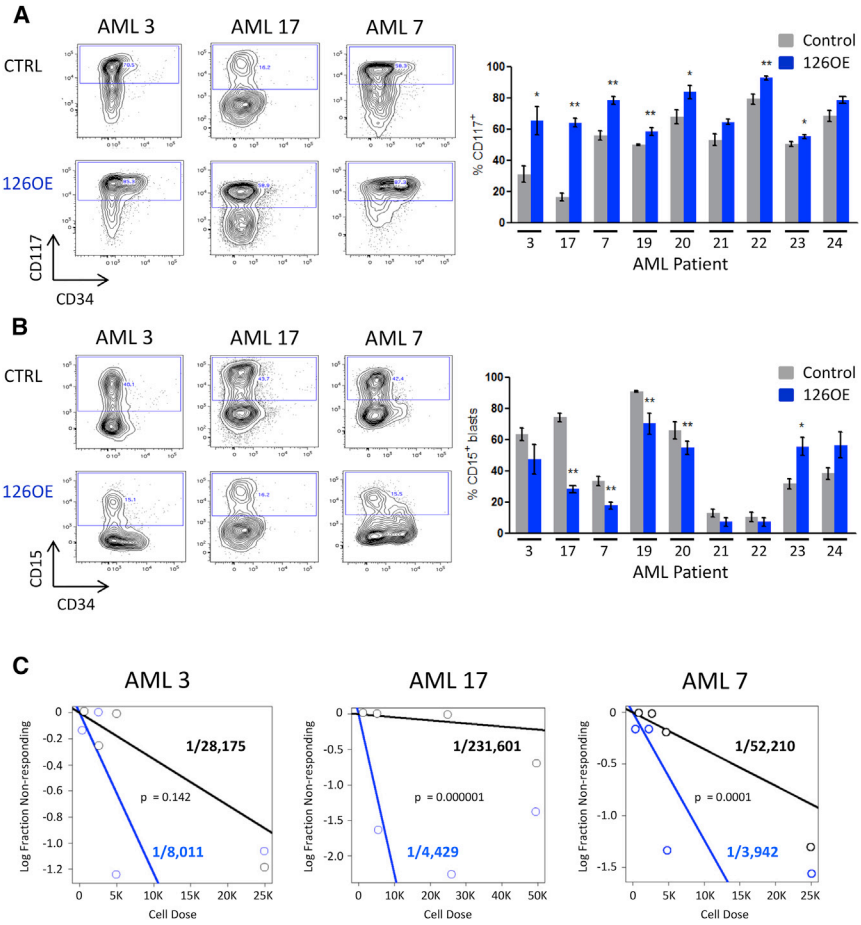

Figure 4. Enforced Expression of miR-126 Expands Primary AML LSC

(A) Representative flow plots depicting changes in CD117$^+$ and CD34$^+$ levels upon 126OE and quantification of the percentage of CD117$^+$ cells within the human CD45$^+$mO+$^+$ graft.

(B) Representative flow plots depicting changes in the percentage of CD34$^+$ and CD15$^+$ cells within the human CD45$^+$mO$^+$ graft and quantification of changes in the percentage of AML cells expressing differentiation marker CD15. Data in (A) and (B) represent means ± SEM of 4–6 mice; *p < 0.05, **p < 0.01.

(C) CD45$^+$mO$^+$ AML cells were flow sorted from primary mice and transplanted in limiting doses into secondary recipients for 8–10 weeks. Human CD45$^+$ marking of > 0.5% was considered positive for AML engraftment. Human grafts were confirmed to be CD33$^+$CD19$^-$ AML. Limiting dilution analysis was performed using ELDA software. See also Figure S4 and Table S2.

upon 126KD (Figures 5C and S5D). Together, these findings suggest that 126KD produces heterogeneous responses with LSC function and frequency reduced in a subset of AML patients.

PI3K/AKT/MTOR Is Targeted by miR-126 in Primitive AML Cells

An integrated transcriptional and proteomic approach was employed to gain mechanistic insight into miR-126 functioning. Quantitative protein mass spectrometry (MS) was performed on bulk 126OE and CTRL 8227 cells resulting in the identification and quantification of 8,848 and 4,837 proteins, respectively. In parallel, gene expression profiling was undertaken on 126KD, 126OE or CTRL CD34$^+$CD38$^-$, and CD34$^+$CD38$^+$ 8227 cells. Gene set enrichment analysis (GSEA) of the proteomics dataset identified pathways and leading edge genes directly targeted by miR-126. In post-analysis, transcriptomic datasets were correlated with proteomic-modulated pathways (Figure 6A). The most significant pathways identified centered on PI3K/AKT/MTOR signaling, a miR-126 target pathway previously validated in primitive normal human CB cells (Lechman et al., 2012). In addition, the protein MS data revealed a strong quiescence signature (Figure S6A) substantiating the in vitro cell cycle effects (Figures 3 and S3). Additional BrdU labeling studies with miR-126OE and miR-126KD confirmed these cell cycle effects in vivo (Figures S6B and S6C). The proteomic analysis was validated and confirmed by western blot of 8227 cells showing that ADAM9, PIK3R2 (p85beta), and AKT levels are reduced in 126OE groups (Figure 6B). Although AKT is not a predicted miR-126 target, the protein MS data show that all three AKT isoforms are reduced by 126OE (Table S4). In addition, many predicted and validated miR-126 targets are signaling inputs for AKT activity (Martelli et al., 2010). To activate AKT,

represents the AML progenitor compartment. Both green and orange gated CD34$^-$ compartments are devoid of LSC and CFU activity, express CD15 and CD14 differentiation markers, and represent terminally differentiated mature AML blasts.

(B) Relative expression of mature miR-126-3p in 8227 cells 7 days after transduction with lentivectors expressing miR-126 (126OE) or an empty control vector (CTRL) measured by qPCR.

(C) The proportion of CD34$^+$ cells over the time course of culture of 126OE and CTRL cells.

(D) Clonogenic potential of sorted subpopulations of 8227 cells after transduction with CTRL or 126OE vectors plated immediately post-sort.

(E) Percent BrdU incorporation into bulk cultures showing proliferation of CTRL and 126OE transduced 8227 cells over time.

(F) Ki67/Hoechst cell cycle staining of CD34$^+$CD38$^-$ LSC-enriched 8227 cells.

(G and H) Percentage of total CD34$^+$ (G) and primitive CD34$^+$CD38$^-$and CD34$^+$CD38$^+$ progenitor cells (H) at day 8 and day 15 post-sort in vitro in 8227 culture after sponge-mediated miR-126 knockdown.

(I) Day 0 post-sort colony-forming potential of sorted fractions of CTRL and 126KD 8227 cells.

(J) Proliferation measured by BrdU incorporation assay of CTRL or 126KD transduced 8227 cells in vitro.

(K) Cell cycle analysis of CD34$^+$CD38$^-$ 8227 cells measured by Ki67/Hoechst staining.

Data are shown as means ± SEM of three biological replicate experiments. *p < 0.05, **p < 0.01, ***p < 0.001. See also Figure S3.

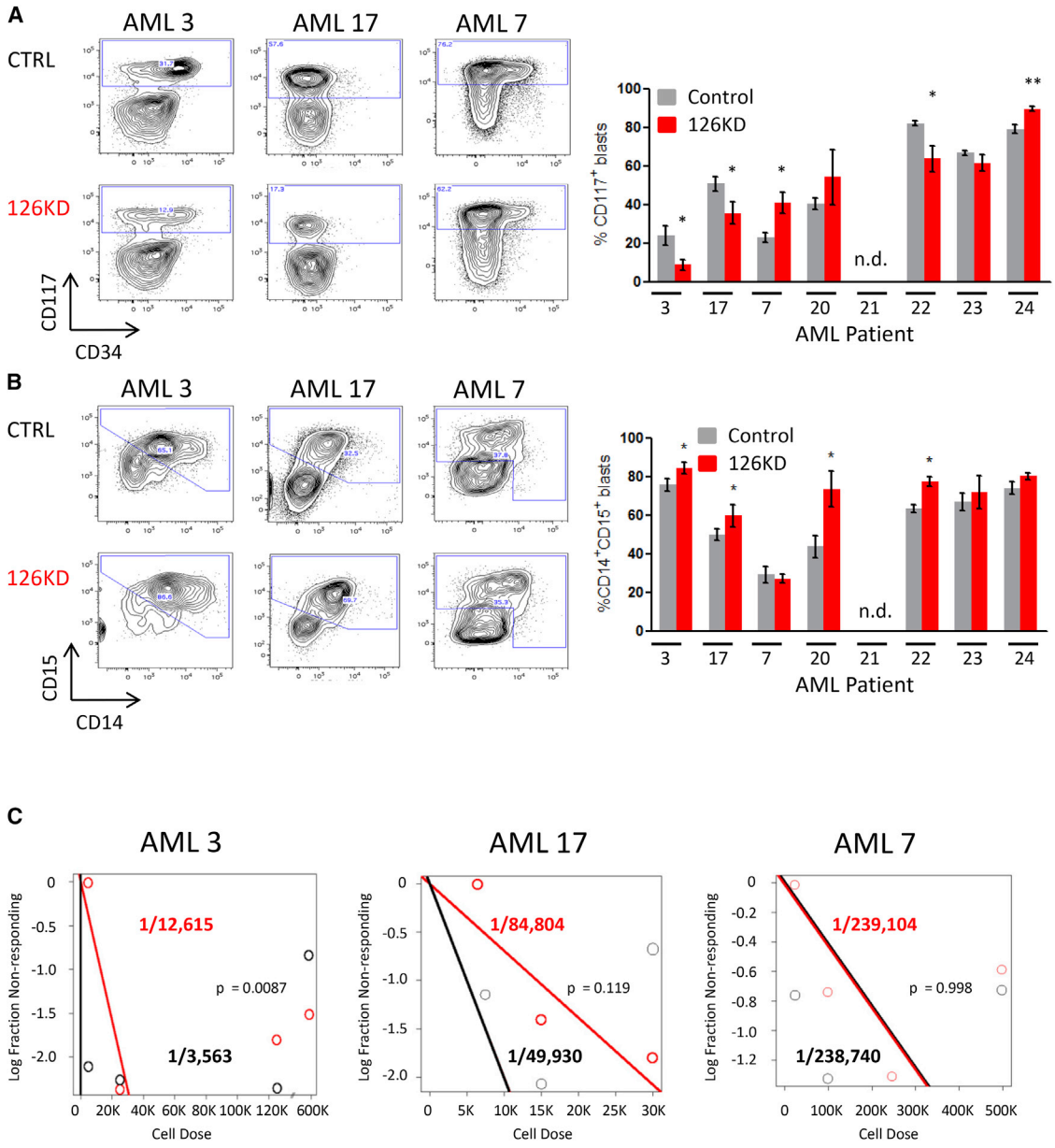

Figure 5. Diminished miR-126 Levels Reduce the Proportion of Primitive AML Cells

(A) Representative flow plots depicting changes in CD117$^+$ and CD34$^+$ levels upon 126KD and quantification of the percentage of CD117$^+$ cells within the human CD45$^+$EGFP$^+$ graft.

(B) Representative flow plots depicting changes in the percentage of CD14$^+$CD15$^+$ cells within the human CD45$^+$EGFP$^+$ graft and quantification of changes in percentage of AML cells expressing differentiation markers CD14 and CD15. Data in (A) and (B) represent means ± SEM of 4–6 mice; *$p < 0.05$, **$p < 0.01$.

(C) CD45$^+$EGFP$^+$ AML cells were flow sorted from primary mice and transplanted at limiting doses into secondary recipients for 8–10 weeks. Human CD45$^+$ marking of >0.5% was considered positive for AML engraftment. Human grafts were confirmed to be CD33$^+$CD19$^-$ AML. Limiting dilution analysis was performed using ELDA software. See also Figure S5.

PDK1 is required to phosphorylate AKT on Thr^{308} in the activation loop. We found that pPDK1 Ser^{241} is reduced with 126OE, suggesting PDK1 activity is reduced by miR-126, further dampening AKT activation (Figure 6C). MTORC2 plays a critical role in AKT Ser^{473} phosphorylation, a prerequisite for full AKT activation. Our proteomics analysis found that MAPKAP1 (Sin1) was downregulated by 126OE (Figure 6A) and since MAPKAP1 is required for MTORC2 complex formation (Yang et al., 2006), its reduction is predicted to reduce MTORC2 activity. Finally, since PTEN antagonizes the PI3K/AKT signaling pathway by dephosphorylating phosphoinositides, and no change in total PTEN levels were observed by protein MS, we checked pPTEN Ser^{380} status and found increased pPTEN Ser^{380} phosphorylation; a modification thought to stabilize PTEN and maintain its

function (Birle et al., 2002). Collectively, this integrated analysis provides strong data that miR-126 expression dampens many components of the PI3K/AKT/MTOR signaling pathway in primitive AML populations.

To characterize miR-126 targets not identified by proteomics or GSEA, all genes upregulated with 126KD and downregulated with 126OE (Figure S6D) were compared in collated lists of predicted miR-126 targets generated from four published prediction algorithms. Genes were ranked according to the level of perturbation by miR-126 (Figure S6E). Selected candidates including ADAM9, ILK, GOLPH3, CDK3, and TOM1 were confirmed as miR-126 targets using 3′ UTR luciferase reporter assays (Figure S6F) (Hamada et al., 2012; Oglesby et al., 2010).

PI3K/AKT signaling ultimately converges upon cyclins and CDK that promote RB1 phosphorylation and cell cycle entry. The uncovering of CDK3 as a potential miR-126 target was intriguing as miR-126 reduces cell cycle progression and CDK3 was previously identified as a gatekeeper of G_0-G_1 cell cycle control (Ren and Rollins, 2004). The PI3K/AKT/MTOR pathway regulates CDKN1B ($p27^{kip}$) protein stability by controlling the levels of SKP2, a component of the SCF^{SKP2} ubiquitin ligase complex (Lin et al., 2009). Both chemical inhibition of PI3K or enforced expression of PTEN induces $p27^{kip}$ upregulation in quiescent cells (Collado et al., 2000; Lu et al., 1999) and CDK3 activity is downregulated with transient $p27^{kip}$ expression (Braun et al., 1998; Hsu et al., 2000). To test the hypothesis that miR-126 modulation of PI3K/AKT/MTOR signaling influences LSC function through CDK3, functional studies were undertaken. Intracellular flow cytometry of 8227 cells showed reduced CDK3 protein levels and pRB $Ser^{807/811}$ levels upon 126OE (Figure 6D). CDK3/cyclin C phosphorylation of RB1 on $Ser^{807/811}$ is required to induce cell cycle entry from a quiescent state (G_0 exit) (Ren and Rollins, 2004) (Miyata et al., 2010) To verify that 126OE functions are dependent on CDK3 downregulation, lentiviruses expressing CDK3 or the CDK3 kinase mutant (CDK3mut) were generated (Figure S6G) (van den Heuvel and Harlow, 1993). Compared with CDK3mut, CDK3 significantly increased proliferation and clonogenicity of $CD34^+CD38^-$ and $CD34^+CD38^+$ cells (Figures 6E and 6F), and partially reversed 126OE-induced expansion of $CD34^+$ cells (Figures 6G and S6H). Collectively, these data suggest that miR-126 restricts LSC proliferation partly through targeting CDK3.

High miR-126 Bioactivity Endows LSC with Chemotherapy Resistance

To test whether the induction of LSC quiescence by 126OE is associated with chemotherapy resistance, 126OE or CTRL transduced 8227 cells were exposed to increasing concentrations of daunorubicin. 126OE increased the survival of $CD34^+$ cells after 72 hr of treatment compared with CTRL (Figure 7A), an effect not seen in non-transduced cells (Figure S7A). Treatment of primary AML samples (Table S5) with daunorubicin plus cytarabine resulted in enrichment of primitive $CD117^+$ cells (Figure S7B) and increased miR-126 levels in four of five samples (Figure 7B). Thus, primitive AML cells expressing the highest miR-126 levels are also the most resistant to anti-proliferative chemotherapy.

To determine if miR-126 expression could be linked to chemotherapy resistance in a clinical setting, biobanked samples were identified from eight AML patients who failed to achieve complete remission after induction therapy. $CD45^{dim}$ blasts were isolated from bone marrow at diagnosis (n = 8, day 0), day 14 (n = 4), and day 30 (n = 5) post-induction, and at day 30 after salvage chemotherapy (n = 3). In line with the in vitro findings, miR-126 expression was increased in six of eight samples (median, 3.4-fold; range, 0.3–9.4) after induction, and in two of three patients (including one in whom miR-126 expression was unchanged after induction) following salvage chemotherapy (median, 1.8-fold; range, 1.1–2.1) (Figures 7C and S7C). miR-126 expression was higher in relapse blasts compared with paired diagnostic samples in all four patients tested (Figures 7D and S7D). miR-126 expression in primitive $CD45^{dim}CD117^+$ cells was increased in eight of ten patients at relapse, with >100-fold enrichment in two patients (Figures 7E and S7E). Finally, enforced expression of CDK3 in 8227 cells rescued the 126OE effects by decreasing the proportion of $CD34^+$ cells resistant to daunorubicin and cytarabine (Figure 7F). Overall, these data suggest that miR-126 confers resistance to chemotherapy, likely through the induction and maintenance of cellular quiescence by the targeting and repression of the PI3K/AKT/MTOR pathway.

DISCUSSION

Our study establishes that miRNAs play a powerful role in governing the fundamental properties that define the stemness state of human LSC including quiescence, self-renewal, and chemotherapy response. miRNAs are differentially expressed within distinct cellular subsets that make up the AML hierarchy, with a restricted set expressed in an LSC-specific manner. The miRNA LSC signature was itself highly prognostic. This clinical association, together with the miR-126 functional data, establishes that miRNAs provide a layer of post-transcriptional control critical for maintaining the stemness state in AML. Although miR-126 governs the stemness and quiescence properties of both HSC and LSC, miR-126 perturbation results in divergent self-renewal outcomes. This discordance provides a novel avenue to therapeutically target LSC without attendant toxicity to HSC.

Our study provides a mechanistic link between quiescence control and the restraint of CDK3 expression by miR-126, thereby altering RB1 phosphorylation and delaying G_0 exit in human primitive AML populations. Regulation of G_0 exit kinetics is a fundamental HSC property, distinct from downstream progenitors, that is essential for maintaining HSC pool integrity (Laurenti et al., 2015; Nygren et al., 2006). CDK3 is poorly studied since all inbred mice carry a nonsense mutation in CDK3 (Ye et al., 2001). In quiescent human fibroblasts, CDK3 can complex with CCNC (cyclin C) and phosphorylate Rb1 (on residues S^{807} and S^{811}) to directly initiate the cell cycle; when CDK3 levels are reduced, a 12-hr lag in G_0 exit kinetics is induced but not a permanent block (Ren and Rollins, 2004). In murine LT-HSC, CCNC levels are highest during G_0 exit (Passegué et al., 2005) and CCNC knockdown in human HSC increased quiescence, promoted HSPC expansion, and increased repopulation capacity (Miyata et al., 2010). In leukemia, CCNC deletion highly correlates with relapse (van Delft et al., 2011). Thus, it is likely that the miR-126/CDK3 regulatory axis also governs G_0 exit kinetics in LSC, thereby providing new therapeutic opportunities for targeting quiescence control of LSC.

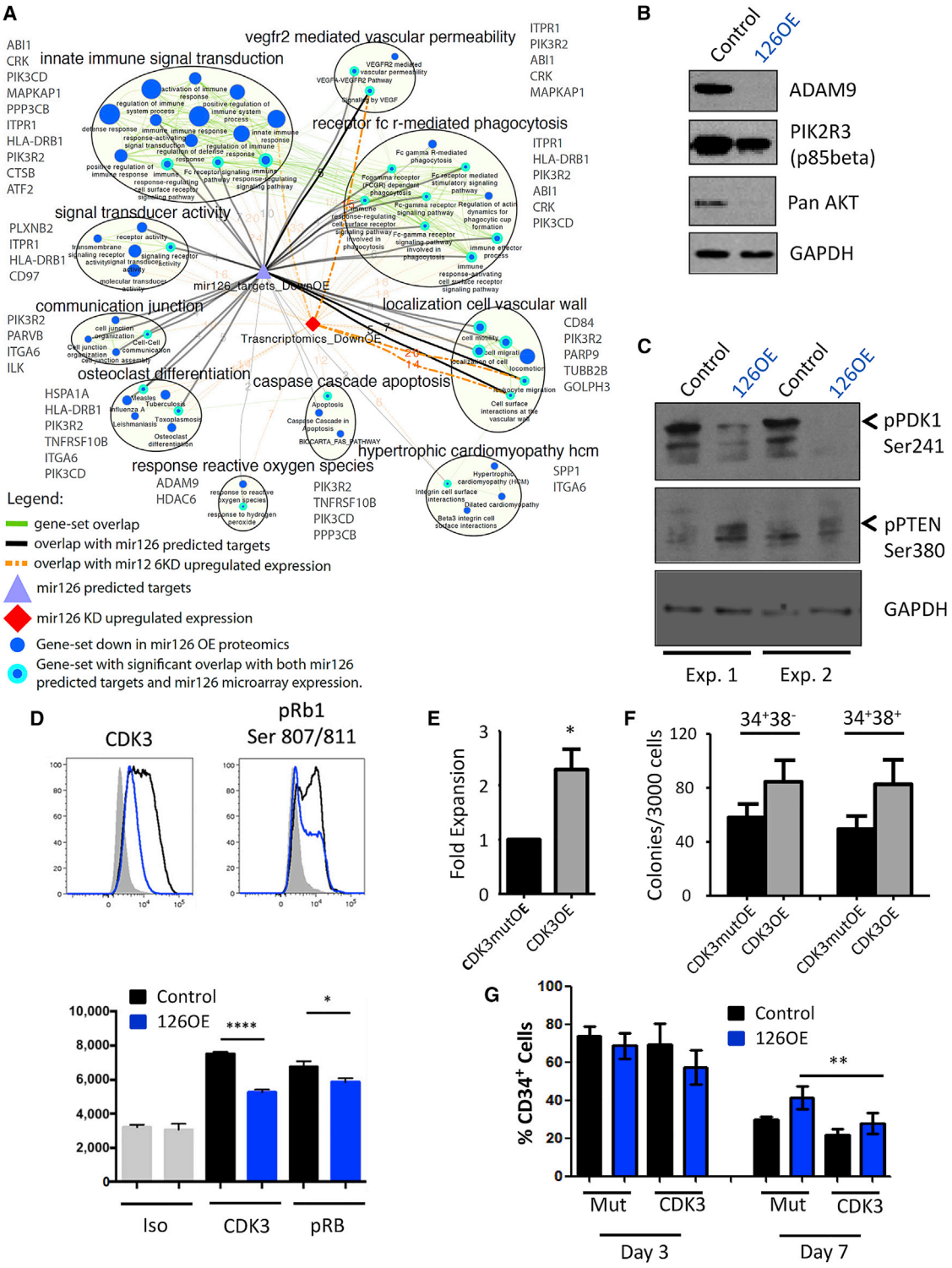

Figure 6. PI3K/AKT/MTOR Is Targeted by miR-126 in Primitive AML Cells

(A) Functional enrichment map for protein MS-based expression revealing miR-126 modulated pathways. Blue nodes (circles) represent gene sets enriched in proteins downregulated in 8227 cells overexpressing miR-126. Green line (edge) width between nodes corresponds to the number of shared proteins. Predicted miR-126 targets (purple triangle) are connected to enriched pathways by gray edges and edge width is proportional to the overlap significance (Wilcoxon proteomics $p < 0.05$ and hypergeometric test $p < 0.05$). Downregulated genes from the transcriptomics data (red diamond) are connected to enriched pathways by orange edges (Wilcoxon proteomics $p < 0.05$, Wilcoxon transcriptomic $p < 0.25$, and hypergeometric $p < 0.05$). Thickest orange and gray edges have significant Wilcoxon and Fisher's exact test $p < 0.05$. Map includes only nodes (cyan border) that have significant overlap with miR-126 predicted targets and

(legend continued on next page)

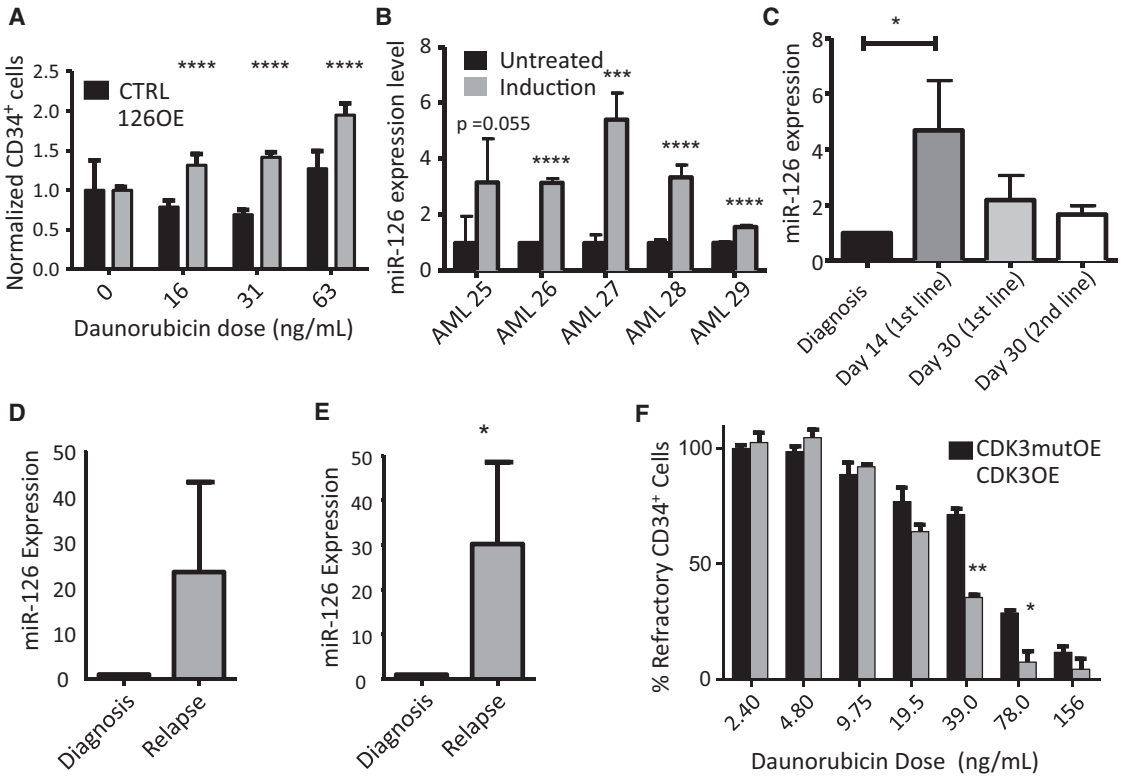

Figure 7. High miR-126 Bioactivity Endows LSC with Chemotherapy Resistance

(A) Graphical representation of percent viable CD34$^+$ 8227 cells with increasing doses of daunorubicin. CD34$^+$ cell numbers were normalized to day 0 control transduced cells. Results are shown as the mean ± SEM of three biological replicate experiments; ****p < 0.0001.

(B) Primary patient AML cells were plated onto MS5 stroma; after 24 hr cells were treated with vehicle or with daunorubicin (50 ng/ml)/AraC (500 ng/ml) for 72 hr. The miR-126 expression levels in daunorubicin/AraC-treated and control AML blasts were determined by qPCR. Results were normalized to RNU48 and are shown as the mean ± SD of four replicates; ***p < 0.001, ****p < 0.0001.

(C) qPCR was performed on CD45^{dim} sorted blasts from patient samples at diagnosis (n = 8, day 0) and at day 14 (n = 4) and day 30 (n = 5) after initiation of induction chemotherapy, as well as on day 30 after (unsuccessful) salvage chemotherapy (n = 3). Data shown are pooled from individual patients (see Figure S7C) and are shown as means ± SEM of combined individual patient samples. *p < 0.05.

(D and E) qPCR results of the relative levels of miR-126 in CD45^{dim} (D, four AML patients, see Figure S7D) and CD45^{dim}CD117$^+$ (E, ten AML patients, see Figure S7E). AML blasts in paired diagnosis and relapse patient samples shown as the mean ± SEM of all patients combined; *p < 0.05.

(F) 8227 cells transduced with mutCDK3 and CDK3 lentiviruses were plated into a 96-well plate and treated with increasing doses of daunorubicin for 48 hr. Cells were stained for CD34 and live cells were identified by viability dye exclusion by flow cytometry. Results are shown as the mean ± SEM of four biological replicates; *p < 0.05 and **p < 0.01. See also Figure S7 and Table S4.

A model derived from our proteomic and transcriptomic data (Figure 8) depicts that upstream of CDK3, miR-126 represses multiple inputs converging on PI3K/AKT/MTOR signaling in LSC, paralleling miR-126 function in HSC (Lechman et al., 2012). Preclinical evidence indicates that activated PI3K/AKT/MTOR signaling plays a role in AML (Martelli et al., 2010) despite

expression data and connected nodes belonging to same clusters (MCL cluster algorithm called from ClusterMaker2). Gene names in gray beside each cluster are the genes that are found in the specified cluster and overlap with predicted miR-126 targets repressed in 126OE.

(B) Western blot of ADAM9, PIK3R2, and AKT levels in 8227 cells transduced with miR-126OE or control lentivirus. GAPDH is the loading control.

(C) Western blot of phospho-PDK1 Ser^{241} and phospho-PTEN Ser^{280} levels in 8227 cells transduced with miR-126OE or control lentivirus. GAPDH is the loading control.

(D) Representative intracellular flow plots for the detection of CDK3 and pRB Ser$^{807/811}$. Graph below represents three independent intracellular flow experiments for each condition where the mean fluorescence intensity was compared. Mean ± SEM; *p=<0.05 and ****p=<0.0001.

(E) Graph depicting enhanced expansion of bulk 8227 cultures after enforced expression of CDK3 and mutCDK3. Fold expansion is normalized to mutCDK3 control culture day 7 after transduction. Data shown are the mean ± SEM of three replicate experiments; *p=<0.05.

(F) Graph showing clonogenic potential of primitive AML cells after enforced expression of CDK3 and mutCDK3. Colony counts are shown as the mean ± SEM of three replicate experiments.

(G) Graph depicting CDK3/OE rescue of CD34$^+$ cell expansion upon 126OE. 8227 cells were transduced with miR-126, and CD34$^+$CD38$^-$ cells were sorted and placed into culture. Cells were transduced with viral vectors expressing the mutCDK3 control vector or CDK3 vector. Flow cytometry was performed at day 3 and day 7. The percentage of CD34$^+$ cells in double-transduced cultures is shown as the mean ± SEM of three replicate experiments, where **p < 0.01. See also Figure S6 and Table S3.

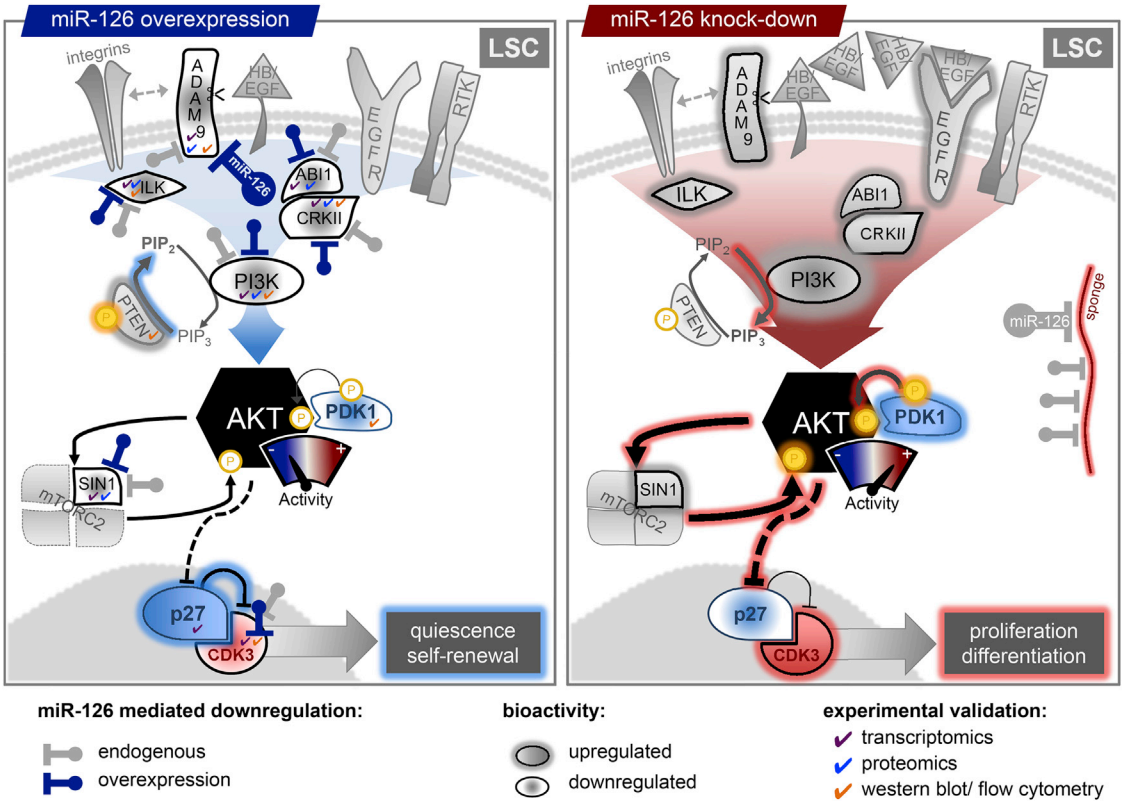

Figure 8. miR-126 Represses Multiple AKT Inputs in LSC

LSC express high endogenous levels of miR-126 compared with more differentiated AML populations. High levels of endogenous or experimental miR-126 repress the level of several proteins regulating AKT (PI3K signaling, PI3CD, PIK3R2; integrin signaling, ADAM9, ITGA6, ILK, PARVB; RTK signaling, CRK, ABI1, CD97, CD84; MTOR signaling, MAPKAP1), reducing overall AKT levels and activity. Furthermore, high levels of miR-126 reduce pPDK1 Ser^{241}, which phosphorylates AKT, and MAPKAP1, which is required for MTORC2 formation and full activation of AKT. Significantly diminished levels of AKT activity preferentially retain LSC in a quiescent state by increasing p27 levels, together with miR-126 targeted reduction of CDK3. Under high miR-126 levels, LSC that do enter the cycle are biased toward a self-renewal division. Reduction of LSC miR-126 levels through currently unspecified developmental cues (or lentiviral sponge-mediated) de-represses the expression and activity of multiple AKT signaling inputs. LSC now preferentially cycle and are biased toward differentiation divisions.

being rarely mutated and likely driven by upstream activation (Fransecky et al., 2015). Although inhibitors of AKT, MTOR, and PI3K are in clinical development, they have mostly failed for AML (Fransecky et al., 2015). While failure is attributed to feedback loops, our study provides an explanation that is embedded in the hierarchical organization of AML. PI3K/AKT/MTOR signaling is restricted to cycling leukemic progenitors; by contrast, quiescent LSC, a reservoir of leukemic relapse, have lower signaling and would then be spared following inhibitor treatment. In support of this prediction, AKT inhibition increased the fraction of G_0 breast cancer cells, linking low AKT signaling to a G_0-like state (Dey-Guha et al., 2011). In AKT knockout mice, HSC persisted in an enhanced G_0 quiescent state, while AKT activation results in HSC hyper-proliferation and exhaustion (Juntilla et al., 2010; Kharas et al., 2010). Collectively, these reports suggest that the state of AKT activity plays a key role in governing quiescence of normal HSC and our data extend this concept to leukemia by showing that this pathway is tightly controlled at multiple points by miRNAs in order to maintain the human LSC state.

Although cell cycle regulation by miR-126 is similar between HSC and LSC, the functional consequence is the opposite: reduced miR-126 levels expand HSC in vivo, but impair LSC maintenance (see the model in Figure 8). With the exception of PTEN, known regulators of self-renewal have similar functions in normal and leukemic contexts (Yilmaz and Morrison, 2008). PTEN is rarely mutated in AML, yet experimental deletion results in HSC loss and LSC expansion, supporting our data on functional HSC–LSC divergence. Concordant with our findings of low PI3K/AKT/MTOR signaling in dormant LSC, rapamycin treatment only eliminates LSC during the early phases of leukemic initiation in PTEN mouse models when LSC are proliferating, but not when leukemia is fully developed and when some LSC are predicted to re-enter quiescence (Yilmaz and Morrison, 2008).

While targeting stemness represents a promising clinical direction, finding a selective therapeutic window might be challenging due to the shared determinants of stemness between HSC and LSC, and the likelihood of causing excessive toxicity (Kreso and Dick, 2014). The distinct function of miR-126 in HSC and LSC provides an opportunity to clinically target LSC while sparing HSC. Moreover, inhibiting miR-126 might overcome LSC chemoresistance through cycle activation and increasing sensitivity to anti-proliferative drugs. Although targeting miRNA in vivo is still

inefficient (Brown and Naldini, 2009), LNA miRNA decoy technology is effective clinically in hepatitis C (Janssen et al., 2013). Alternatively, targeting the LSC-specific pathways identified by miR-126 might also be an effective strategy.

EXPERIMENTAL PROCEDURES

Patient-Derived Xenografts

NOD/Lt-scid/IL2Rγnull (NSG) mice were bred at the University Health Network/Princess Margaret Cancer Center. Animal experiments were performed in accordance with national and institutional guidelines approved by the Canadian Counsel on Animal Care and approved by the University Health Network Animal Care Committee. Mouse xenografts were performed as described previously (Lechman et al., 2012). Briefly, NSG mice were sublethally irradiated (225 cGy) 1 day prior to injection. AML patient samples were thawed and plated in X-VIVO/20% BIT (Stem Cell Technologies) supplemented with Flt3-L (50 ng/ml), IL-6 (10 ng/ml), stem cell factor (50 ng/ml), thrombopoietin (125 ng/ml), IL-3 (10 ng/ml), granulocyte colony-stimulating factor (10 ng/ml) for 18 hr (Blair et al., 1998). Cells were transduced in 24-well culture plates at a multiplicity of infection of 30 with sensor lentivectors or for enforced expression and knockdown of miR-126. Transduced AML cells (5×10^5–1×10^6) were injected with 25 μl of PBS into the right femur of each recipient mouse. After 10–12 weeks, the mice were euthanized and bone marrow cells were flushed with 2 ml of PBS, 2% fetal calf serum, and 50 μl of cells were stained for surface markers.

Patient Samples and Treatment Protocols

Between 2003 and 2010, peripheral blood and bone marrow samples were collected from subjects with AML after obtaining informed consent according to procedures approved by the Research Ethics Board of the University Health Network (REB# 01-0573-C). Mononuclear cells were isolated and stored as previously described (Eppert et al., 2011). Cytogenetics were analyzed according to the revised MRC prognostic classification system (Grimwade et al., 2010). *NPM1* and *FLT3*-ITD mutations were assessed as previously described (How et al., 2012).

The 74 patient samples used to optimize the miRNA prognostic signature (PMCC cohort) were diagnostic samples from individuals with de novo AML and normal cytogenetics. Although patients were not treated uniformly, all initially received induction chemotherapy followed by two cycles of consolidation in those who achieved complete remission (CR). First-line induction regimens included 3 + 7 (n = 69), NOVE-HIDAC (n = 1), and four patients were enrolled in clinical trials employing a 3 + 7 backbone with gemtuzumab ozogamicin (n = 2) or tipifarnib (n = 2). Treatment protocols were as previously described (Brandwein et al., 2008; Brandwein et al., 2009; How et al., 2012; Petersdorf et al., 2013). Allogeneic stem cell transplant (allo-SCT) was performed for high-risk patients in CR1 (n = 7), as well as for patients who achieved a second remission after relapse (n = 12) if they had an available donor, were younger than 70 years, lacked significant comorbidities, and had good performance status. Bio-informatic and clinical information for a second cohort of 187 de novo AML patients was obtained from TCGA and has been previously described (Cancer Genome Atlas Research Network, 2013).

See Supplemental Experimental Procedures for additional methods.

ACCESSION NUMBERS

miRNA array, Illumina array, Nanostring data have been submitted to Gene Expression Omnibus (http://www.ncbi.nlm.nih.gov/geo) with the following series accession numbers: miRNA, GEO: GSE55917; Illumina, GEO: GSE55814; and Nanostring, GEO: GSE55770. The MS data have been deposited in the ProteomeXchange Consortium (http://proteomecentral.proteomexchange.org) via the PRIDE partner repository with the dataset identifier PRIDE: PXD001994.

SUPPLEMENTAL INFORMATION

Supplemental Information includes Supplemental Experimental Procedures, seven figures, and five tables and can be found with this article online at http://dx.doi.org/10.1016/j.ccell.2015.12.011.

AUTHOR CONTRIBUTIONS

Project Conceptualization, E.R.L, B.G., J.E.D., L.N, K.E., M.M., and J.C.Y.W.; Methodology, E.R.L. and K.E.; Investigation, E.R.L., E.M.S., P.V.G., N.T., S.M.D., A.T.G., G.K., J.E., A.M., W.C.C., K.G.H., K.E., R.M., B.L.E., J.L., and S.N.; Resources, M.M.; Data Curation, J.K.; Writing-Review and Editing, E.R.L. J.C.Y.W., and J.E.D.; Supervision, J.E.D., L.N., G.D.B., P.Z., and T.G.; Formal Analysis, S.W.K.N., J.K., B.N., R.I., V.V.; Visualization, K.K.; Funding Acquisition, T.G., J.E.D., and L.N.

ACKNOWLEDGMENTS

We thank Dr. M Roehrl for mass spectrometer support, A Khandani and P. A. Penttilä for flow cytometry, and the Dick and Naldini laboratories for critical review. This work was supported by grants to L.N. from Telethon (TIGET grant), EU (FP7 GA 222878 PERSIST, ERC Advanced Grant 249845 TARGETING GENE THERAPY), and the Italian Ministry of Health and to J.E.D. from the Canadian Institutes for Health Research, Canadian Cancer Society, Terry Fox Foundation, Genome Canada through the Ontario Genomics Institute, Ontario Institute for Cancer Research with funds from the Province of Ontario, and a Canada Research Chair. E.M.S. is an EMBO Postdoctoral Fellow (ALTF 1595–2014) and is co-funded by the European Commission (LTFCOFUND2013, GA-2013-609409) and Marie Curie Actions. This research was funded in part by the Ontario Ministry of Health and Long Term Care (OMOHLTC). The views expressed do not necessarily reflect those of the OMOHLTC.

Received: March 17, 2014
Revised: July 13, 2015
Accepted: December 21, 2015
Published: January 28, 2016

REFERENCES

Birle, D., Bottini, N., Williams, S., Huynh, H., deBelle, I., Adamson, E., and Mustelin, T. (2002). Negative feedback regulation of the tumor suppressor PTEN by phosphoinositide-induced serine phosphorylation. J. Immunol. *1950*, 286–291.

Blair, A., Hogge, D.E., and Sutherland, H.J. (1998). Most acute myeloid leukemia progenitor cells with long-term proliferative ability in vitro and in vivo have the phenotype CD34+/CD71−/HLA-DR−. Blood *92*, 4325–4335.

Brandwein, J.M., Gupta, V., Schuh, A.C., Schimmer, A.D., Yee, K., Xu, W., Messner, H.A., Lipton, J.H., and Minden, M.D. (2008). Predictors of response to reinduction chemotherapy for patients with acute myeloid leukemia who do not achieve complete remission with frontline induction chemotherapy. Am. J. Hematol. *83*, 54–58.

Brandwein, J.M., Leber, B.F., Howson-Jan, K., Schimmer, A.D., Schuh, A.C., Gupta, V., Yee, K.W.L., Wright, J., Moore, M., MacAlpine, K., et al. (2009). A phase I study of tipifarnib combined with conventional induction and consolidation therapy for previously untreated patients with acute myeloid leukemia aged 60 years and over. Leukemia *23*, 631–634.

Braun, K., Hölzl, G., Soucek, T., Geisen, C., Möröy, T., and Hengstschläger, M. (1998). Investigation of the cell cycle regulation of cdk3-associated kinase activity and the role of cdk3 in proliferation and transformation. Oncogene *17*, 2259–2269.

Brown, B.D., and Naldini, L. (2009). Exploiting and antagonizing microRNA regulation for therapeutic and experimental applications. Nat. Rev. Genet. *10*, 578–585.

Cancer Genome Atlas Research Network. (2013). Genomic and epigenomic landscapes of adult de novo acute myeloid leukemia. N. Engl. J. Med. *368*, 2059–2074.

Collado, M., Medema, R.H., Garcia-Cao, I., Dubuisson, M.L., Barradas, M., Glassford, J., Rivas, C., Burgering, B.M., Serrano, M., and Lam, E.W. (2000). Inhibition of the phosphoinositide 3-kinase pathway induces a senescence-like arrest mediated by p27Kip1. J. Biol. Chem. *275*, 21960–21968.

Dey-Guha, I., Wolfer, A., Yeh, A.C., G Albeck, J., Darp, R., Leon, E., Wulfkuhle, J., Petricoin, E.F., Wittner, B.S., and Ramaswamy, S. (2011). Asymmetric cancer cell division regulated by AKT. Proc. Natl. Acad. Sci. USA *108*, 12845–12850.

Dorrance, A.M., Neviani, P., Ferenchak, G.J., Huang, X., Nicolet, D., Maharry, K.S., Ozer, H.G., Hoellarbauer, P., Khalife, J., Hill, E.B., et al. (2015). Targeting leukemia stem cells in vivo with antagomiR-126 nanoparticles in acute myeloid leukemia. Leukemia *29*, 2143–2153.

de Leeuw, D.C., Denkers, F., Olthof, M., Rutten, A., Pouwels, W., Schuurhuis, G.J., Ossenkoppele, G., and Smit, L. (2014). Attenuation of microRNA-126 expression that drives CD34+38- stem/progenitor cells in acute myeloid leukemia leads to tumor eradication. Cancer Res. *74*, 2094–2105.

Ebert, M.S., and Sharp, P.A. (2012). Roles for microRNAs in conferring robustness to biological processes. Cell *149*, 515–524.

Eppert, K., Takenaka, K., Lechman, E.R., Waldron, L., Nilsson, B., van Galen, P., Metzeler, K.H., Poeppl, A., Ling, V., Beyene, J., et al. (2011). Stem cell gene expression programs influence clinical outcome in human leukemia. Nat. Med. *17*, 1086–1093.

Fransecky, L., Mochmann, L.H., and Baldus, C.D. (2015). Outlook on PI3K/AKT/mTOR inhibition in acute leukemia. Mol. Cell. Ther. *3*, 2.

Garzon, R., Volinia, S., Liu, C.-G., Fernandez-Cymering, C., Palumbo, T., Pichiorri, F., Fabbri, M., Coombes, K., Alder, H., Nakamura, T., et al. (2008). MicroRNA signatures associated with cytogenetics and prognosis in acute myeloid leukemia. Blood *111*, 3183–3189.

Gentner, B., Visigalli, I., Hiramatsu, H., Lechman, E., Ungari, S., Giustacchini, A., Schira, G., Amendola, M., Quattrini, A., Martino, S., et al. (2010). Identification of hematopoietic stem cell-specific miRNAs enables gene therapy of globoid cell leukodystrophy. Sci. Transl. Med. *2*, 58ra84.

Greaves, M. (2011). Cancer stem cells renew their impact. Nat. Med. *17*, 1046–1048.

Grimwade, D., Hills, R.K., Moorman, A.V., Walker, H., Chatters, S., Goldstone, A.H., Wheatley, K., Harrison, C.J., Burnett, A.K., and National Cancer Research Institute Adult Leukaemia Working Group. (2010). Refinement of cytogenetic classification in acute myeloid leukemia: determination of prognostic significance of rare recurring chromosomal abnormalities among 5876 younger adult patients treated in the United Kingdom Medical Research Council trials. Blood *116*, 354–365.

Guo, S., Lu, J., Schlanger, R., Zhang, H., Wang, J.Y., Fox, M.C., Purton, L.E., Fleming, H.H., Cobb, B., Merkenschlager, M., et al. (2010). MicroRNA miR-125a controls hematopoietic stem cell number. Proc. Natl. Acad. Sci. USA *107*, 14229–14234.

Hamada, S., Satoh, K., Fujibuchi, W., Hirota, M., Kanno, A., Unno, J., Masamune, A., Kikuta, K., Kume, K., and Shimosegawa, T. (2012). MiR-126 acts as a tumor suppressor in pancreatic cancer cells via the regulation of ADAM9. Mol. Cancer Res. *10*, 3–10.

Han, Y.-C., Park, C.Y., Bhagat, G., Zhang, J., Wang, Y., Fan, J.-B., Liu, M., Zou, Y., Weissman, I.L., and Gu, H. (2010). microRNA-29a induces aberrant self-renewal capacity in hematopoietic progenitors, biased myeloid development, and acute myeloid leukemia. J. Exp. Med. *207*, 475–489.

Holtz, M., Forman, S.J., and Bhatia, R. (2007). Growth factor stimulation reduces residual quiescent chronic myelogenous leukemia progenitors remaining after imatinib treatment. Cancer Res. *67*, 1113–1120.

How, J., Sykes, J., Gupta, V., Yee, K.W.L., Schimmer, A.D., Schuh, A.C., Minden, M.D., Kamel-Reid, S., and Brandwein, J.M. (2012). Influence of FLT3-internal tandem duplication allele burden and white blood cell count on the outcome in patients with intermediate-risk karyotype acute myeloid leukemia. Cancer *118*, 6110–6117.

Hsu, S.L., Hsu, J.W., Liu, M.C., Chen, L.Y., and Chang, C.D. (2000). Retinoic acid-mediated G1 arrest is associated with induction of p27(Kip1) and inhibition of cyclin-dependent kinase 3 in human lung squamous carcinoma CH27 cells. Exp. Cell Res. *258*, 322–331.

Hu, W., Dooley, J., Chung, S.S., Chandramohan, D., Cimmino, L., Mukherjee, S., Mason, C.E., de Strooper, B., Liston, A., and Park, C.Y. (2015). miR-29a maintains mouse hematopoietic stem cell self-renewal by regulating Dnmt3a. Blood *125*, 2206–2216.

Janssen, H.L.A., Reesink, H.W., Lawitz, E.J., Zeuzem, S., Rodriguez-Torres, M., Patel, K., van der Meer, A.J., Patick, A.K., Chen, A., Zhou, Y., et al. (2013). Treatment of HCV infection by targeting microRNA. N. Engl. J. Med. *368*, 1685–1694.

Juntilla, M.M., Patil, V.D., Calamito, M., Joshi, R.P., Birnbaum, M.J., and Koretzky, G.A. (2010). AKT1 and AKT2 maintain hematopoietic stem cell function by regulating reactive oxygen species. Blood *115*, 4030–4038.

Kharas, M.G., Okabe, R., Ganis, J.J., Gozo, M., Khandan, T., Paktinat, M., Gilliland, D.G., and Gritsman, K. (2010). Constitutively active AKT depletes hematopoietic stem cells and induces leukemia in mice. Blood *115*, 1406–1415.

Kreso, A., and Dick, J.E. (2014). Evolution of the cancer stem cell model. Cell Stem Cell *14*, 275–291.

Laurenti, E., Frelin, C., Xie, S., Ferrari, R., Dunant, C.F., Zandi, S., Neumann, A., Plumb, I., Doulatov, S., Chen, J., et al. (2015). CDK6 levels regulate quiescence exit in human hematopoietic stem cells. Cell Stem Cell *16*, 302–313.

Lechman, E.R., Gentner, B., van Galen, P., Giustacchini, A., Saini, M., Boccalatte, F.E., Hiramatsu, H., Restuccia, U., Bachi, A., Voisin, V., et al. (2012). Attenuation of miR-126 activity expands HSC in vivo without exhaustion. Cell Stem Cell *11*, 799–811.

Li, Z., Lu, J., Sun, M., Mi, S., Zhang, H., Luo, R.T., Chen, P., Wang, Y., Yan, M., Qian, Z., et al. (2008). Distinct microRNA expression profiles in acute myeloid leukemia with common translocations. Proc. Natl. Acad. Sci. USA *105*, 15535–15540.

Lin, H.-K., Wang, G., Chen, Z., Teruya-Feldstein, J., Liu, Y., Chan, C.-H., Yang, W.-L., Erdjument-Bromage, H., Nakayama, K.I., Nimer, S., et al. (2009). Phosphorylation-dependent regulation of cytosolic localization and oncogenic function of Skp2 by Akt/PKB. Nat. Cell Biol. *11*, 420–432.

Lu, Y., Lin, Y.Z., LaPushin, R., Cuevas, B., Fang, X., Yu, S.X., Davies, M.A., Khan, H., Furui, T., Mao, M., et al. (1999). The PTEN/MMAC1/TEP tumor suppressor gene decreases cell growth and induces apoptosis and anoikis in breast cancer cells. Oncogene *18*, 7034–7045.

Marcucci, G., Radmacher, M.D., Mrózek, K., and Bloomfield, C.D. (2009). MicroRNA expression in acute myeloid leukemia. Curr. Hematol. Malig. Rep. *4*, 83–88.

Martelli, A.M., Evangelisti, C., Chiarini, F., and McCubrey, J.A. (2010). The phosphatidylinositol 3-kinase/Akt/mTOR signaling network as a therapeutic target in acute myelogenous leukemia patients. Oncotarget *1*, 89–103.

Mehta, A., Zhao, J.L., Sinha, N., Marinov, G.K., Mann, M., Kowalczyk, M.S., Galimidi, R.P., Du, X., Erikci, E., Regev, A., et al. (2015). The Microrna-132 and MicroRNA-212 cluster regulates hematopoietic stem cell maintenance and survival with age by buffering FOXO3 expression. Immunity *42*, 1021–1032.

Metzeler, K.H., Maharry, K., Kohlschmidt, J., Volinia, S., Mrózek, K., Becker, H., Nicolet, D., Whitman, S.P., Mendler, J.H., Schwind, S., et al. (2013). A stem cell-like gene expression signature associates with inferior outcomes and a distinct microRNA expression profile in adults with primary cytogenetically normal acute myeloid leukemia. Leukemia *27*, 2023–2031.

Miyata, Y., Liu, Y., Jankovic, V., Sashida, G., Lee, J.M., Shieh, J.-H., Naoe, T., Moore, M., and Nimer, S.D. (2010). Cyclin C regulates human hematopoietic stem/progenitor cell quiescence. Stem Cells *28*, 308–317.

Nygren, J.M., Bryder, D., and Jacobsen, S.E.W. (2006). Prolonged cell cycle transit is a defining and developmentally conserved hemopoietic stem cell property. J. Immunol. *177*, 201–208.

Oglesby, I.K., Bray, I.M., Chotirmall, S.H., Stallings, R.L., O'Neill, S.J., McElvaney, N.G., and Greene, C.M. (2010). miR-126 is downregulated in cystic fibrosis airway epithelial cells and regulates TOM1 expression. J. Immunol. *184*, 1702–1709.

Ooi, A.G.L., Sahoo, D., Adorno, M., Wang, Y., Weissman, I.L., and Park, C.Y. (2010). MicroRNA-125b expands hematopoietic stem cells and enriches for the lymphoid-balanced and lymphoid-biased subsets. Proc. Natl. Acad. Sci. USA *107*, 21505–21510.

O'Connell, R.M., Chaudhuri, A.A., Rao, D.S., Gibson, W.S.J., Balazs, A.B., and Baltimore, D. (2010). MicroRNAs enriched in hematopoietic stem cells differentially regulate long-term hematopoietic output. Proc. Natl. Acad. Sci. USA *107*, 14235–14240.

Passegué, E., Wagers, A.J., Giuriato, S., Anderson, W.C., and Weissman, I.L. (2005). Global analysis of proliferation and cell cycle gene expression in the regulation of hematopoietic stem and progenitor cell fates. J. Exp. Med. *202*, 1599–1611.

Petersdorf, S.H., Kopecky, K.J., Slovak, M., Willman, C., Nevill, T., Brandwein, J., Larson, R.A., Erba, H.P., Stiff, P.J., Stuart, R.K., et al. (2013). A phase 3 study of gemtuzumab ozogamicin during induction and postconsolidation therapy in younger patients with acute myeloid leukemia. Blood *121*, 4854–4860.

Ren, S., and Rollins, B.J. (2004). Cyclin C/cdk3 promotes Rb-dependent G0 exit. Cell *117*, 239–251.

Rodgers, J.T., King, K.Y., Brett, J.O., Cromie, M.J., Charville, G.W., Maguire, K.K., Brunson, C., Mastey, N., Liu, L., Tsai, C.-R., et al. (2014). mTORC1 controls the adaptive transition of quiescent stem cells from G0 to G(Alert). Nature *510*, 393–396.

Schneider, T., Flörcken, A., Singh, A., Türkmen, S., Burmeister, T., Anagnostopoulos, I., Pezzutto, A., Dörken, B., and Westermann, J. (2015). Flow cytometric maturity score as a novel prognostic parameter in patients with acute myeloid leukemia. Ann. Hematol. *94*, 1337–1345.

Song, S.J., Ito, K., Ala, U., Kats, L., Webster, K., Sun, S.M., Jongen-Lavrencic, M., Manova-Todorova, K., Teruya-Feldstein, J., Avigan, D.E., et al. (2013). The oncogenic MicroRNA miR-22 targets the TET2 tumor suppressor to promote hematopoietic stem cell self-renewal and transformation. Cell Stem Cell *13*, 87–101.

Trumpp, A., Essers, M., and Wilson, A. (2010). Awakening dormant haematopoietic stem cells. Nat. Rev. Immunol. *10*, 201–209.

Undi, R.B., Kandi, R., and Gutti, R.K. (2013). MicroRNAs as haematopoiesis regulators. Adv. Hematol. *2013*, 1–20.

van Delft, F.W., Horsley, S., Colman, S., Anderson, K., Bateman, C., Kempski, H., Zuna, J., Eckert, C., Saha, V., Kearney, L., et al. (2011). Clonal origins of relapse in ETV6-RUNX1 acute lymphoblastic leukemia. Blood *117*, 6247–6254.

van den Heuvel, S., and Harlow, E. (1993). Distinct roles for cyclin-dependent kinases in cell cycle control. Science *262*, 2050–2054.

Velu, C.S., Chaubey, A., Phelan, J.D., Horman, S.R., Wunderlich, M., Guzman, M.L., Jegga, A.G., Zeleznik-Le, N.J., Chen, J., Mulloy, J.C., et al. (2014). Therapeutic antagonists of microRNAs deplete leukemia-initiating cell activity. J. Clin. Invest. *124*, 222–236.

Viatour, P., Somervaille, T.C., Venkatasubrahmanyam, S., Kogan, S., McLaughlin, M.E., Weissman, I.L., Butte, A.J., Passegué, E., and Sage, J. (2008). Hematopoietic stem cell quiescence is maintained by compound contributions of the retinoblastoma gene family. Cell Stem Cell *3*, 416–428.

Wong, P., Iwasaki, M., Somervaille, T.C.P., Ficara, F., Carico, C., Arnold, C., Chen, C.-Z., and Cleary, M.L. (2010). The miR-17-92 microRNA polycistron regulates MLL leukemia stem cell potential by modulating p21 expression. Cancer Res. *70*, 3833–3842.

Yang, Q., Inoki, K., Ikenoue, T., and Guan, K.-L. (2006). Identification of Sin1 as an essential TORC2 component required for complex formation and kinase activity. Genes Dev. *20*, 2820–2832.

Ye, X., Zhu, C., and Harper, J.W. (2001). A premature-termination mutation in the Mus musculus cyclin-dependent kinase 3 gene. Proc. Natl. Acad. Sci. USA *98*, 1682–1686.

Yilmaz, O.H., and Morrison, S.J. (2008). The PI-3kinase pathway in hematopoietic stem cells and leukemia-initiating cells: a mechanistic difference between normal and cancer stem cells. Blood Cells. Mol. Dis. *41*, 73–76.

Cancer Cell, Volume *29*

Supplemental Information

miR-126 Regulates Distinct Self-Renewal Outcomes in Normal and Malignant Hematopoietic Stem Cells

Eric R. Lechman, Bernhard Gentner, Stanley W.K. Ng, Erwin M. Schoof, Peter van Galen, James A. Kennedy, Silvia Nucera, Fabio Ciceri, Kerstin B. Kaufmann, Naoya Takayama, Stephanie M. Dobson, Aaron Trotman-Grant, Gabriela Krivdova, Janneke Elzinga, Amanda Mitchell, Björn Nilsson, Karin G. Hermans, Kolja Eppert, Rene Marke, Ruth Isserlin, Veronique Voisin, Gary D. Bader, Peter W. Zandstra, Todd R. Golub, Benjamin L. Ebert, Jun Lu, Mark Minden, Jean C.Y. Wang, Luigi Naldini, and John E. Dick

SUPPLEMENTAL DATA

A

AML	Relapse or Diagnosis	FAB	Age	Sex	Karyotype	Engraftment of AML Subpopulations			
						$CD34^+$ $CD38^-$	$CD34^+$ $CD38^-$	$CD34^-$ $CD38^+$	$CD34^-$ $CD38^-$
1	Relapse	M2	48	F	46, t(2;21)(p21;q22)[4]/46,9(1;21)(q22;q22)	+	+	-	-
2	Diag	M5a	58	F	46, XX	+	+	-	-
3	Diag	unclass	52	F	47, XX, +8	+	+	+	+
4	Diag	unclass	62	M	46, XY	+	+	-	+
5	Diag	M5a	39	F	47, XX,+8	+	+	-	-
6	Diag	unclass	80	F	46, XX	+	+	-	-
7	Diag	M5	48	M	no data	+	NT	NT	+
8	Diag	M1	72	F	46, XX	+	-	-	-
9	Diag	M2	47	F	46,t(2:21)[4]/t(6:21)[2]/t(15:21)[2]	+	NT	NT	NT
10	Diag	M2	62	F	47,XX, +13	+	NT	NT	NT
11	Diag	M1	45	F	46, XX	+	+	-	-
12	Diag	M4eo	39	M	46,inv(16)(p13;q22)	+	-	NT	-
13	Diag	M5a	75	M	46, XX	-	-	-	-
14	Diag	M4	23	M	46, XY	NT	-	-	-
15	Diag	M5a	40	M	46, XY	+	+	-	-
16	Diag	M5b	80	M	no data	NT	-	-	-

B

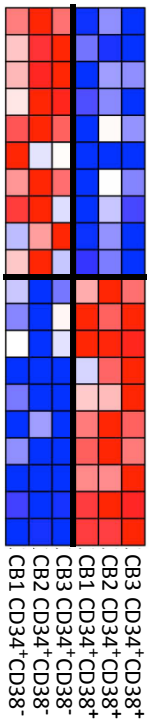

Probe	q value
hsa-miR-10a	0.34
hsa-miR-23b	0.39
hsa-miR-125a-5p	0.51
hsa-miR-342-3p	0.58
hsa-miR-10b hairpin	0.60
hsa-miR-326	0.60
hsa-miR-92b	0.74
hsa-miR-10b	0.76
hsa-miR-92a	0.76
hsa-miR-23a	0.76
hsa-miR-15b	0.59
hsa-miR-let-7d	0.58
hsa-miR-20b	0.58
hsa-miR-128	0.58
hsa-miR-98	0.58
hsa-miR-130b	0.34
hsa-miR-766	0.34
hsa-miR-486-5p	0.13
hsa-miR-20a	0.01
hsa-miR-181c	0.01

C

Population	Probe	q value
$CD34^+/CD38^-$		
	hsa-mmu-let-7b	0.0000
	hsa-mmu-let-7f	0.0138
	hsa-mmu-let-7a	0.0155
	hsa-mmu-miR-326	0.0371
$CD34^+$		
	hsa-mmu-let-7b	0.0000
	hsa-mmu-let-7a	0.0049
	hsa-mmu-let-7c	0.0089
	hsa-mmu-let-7f	0.0181
	hsa-miR-486-5p	0.0854
	hsa-mmu-miR-451	0.0854
	hsa-mmu-542-3p	0.0089
	hsa-miR-299-5p	0.0087
	hsa-mmu-miR-363	0.0013

Population	Probe	q value
BULK		
	hsa-mmu-let-7b	0.0000
	hsa-mmu-miR-425	0.0009
	hsa-mmu-let-7a	0.0061
	hsa-mmu-let-7c	0.0579
	hsa-mmu-miR-221	0.0579
	hsa-miR-520a-5p	0.0986
	hsa-miR-329	0.0885
	hsa-miR-193a-3p	0.0579
	hsa-miR-598	0.0566
	hsa-miR-525-3p	0.0490
	hsa-mmu-miR-26a	0.0325
	hsa-mmu-miR-542-3p	0.0064
	hsa-mmu-miR-186	0.0036
	hsa-miR-202	0.0026
	hsa-miR-299-5p	0.0013
	hsa-mmu-miR-363	0.0006

Figure S1, related to Figure 1. Generation an HSC-enriched miRNA signature and bioinformatic comparison of miRNA enriched in AML and CB fractions.

(A) Table detailing the clinical attributes of 16 AML patient samples used for the generation of a miRNA enriched LSC signature. A (+) denotes a sorted AML fraction the contained leukemia-initiating capacity in vivo, while (-) signifies no such activity was present after transplantation. (NT) indicates fractions that were not tested.

(B) Heat map depicting the top 10 miRNA candidates enriched within the human $CD34^{+}CD38^{-}$ HSC compartment and those enriched within the $CD34^{+}CD38^{+}$ committed hematopoietic progenitor population.

(C) Table of statistically significant miRNA probes enriched in AML (red type) or human lin^{-} CB (blue type) after informatic comparison of normal CB and malignant $CD34^{+}CD38^{-}$, $CD34^{+}$ or bulk cellular populations.

Table S1, related to Figure 1. Clinical and Molecular Characteristics of Patients Analyzed via Nanostring (PMCC Cohort)

	n=74
Male sex [n (%)]	36 (49%)
Age at AML diagnosis [years]	
median (range)	51.4 (23.2-75.9)
WBC count at diagnosis ($x10^9$/L)	
median (range)	18.2 (0.3-207)
% Blasts in PB at diagnosis	
median (range)	57 (0-98)
% Blasts in BM at diagnosis	
median (range)	70 (20-96)
Sample Material	
Bone Marrow [n (%)]	57 (77%)
Peripheral Blood [n (%)]	17 (23%)
Molecular Data [n (%)]	
mutated NPM1 (n=67)	36 (54%)
FLT3-ITD (n=67)	0
Treatment Approach	
Induction	74 (100%)
Allogeneic Transplant	19 (26%)
in CR1	7 (37%)
in CR2	12 (63%)

All samples were from diagnosis and had normal cytogenetics

A

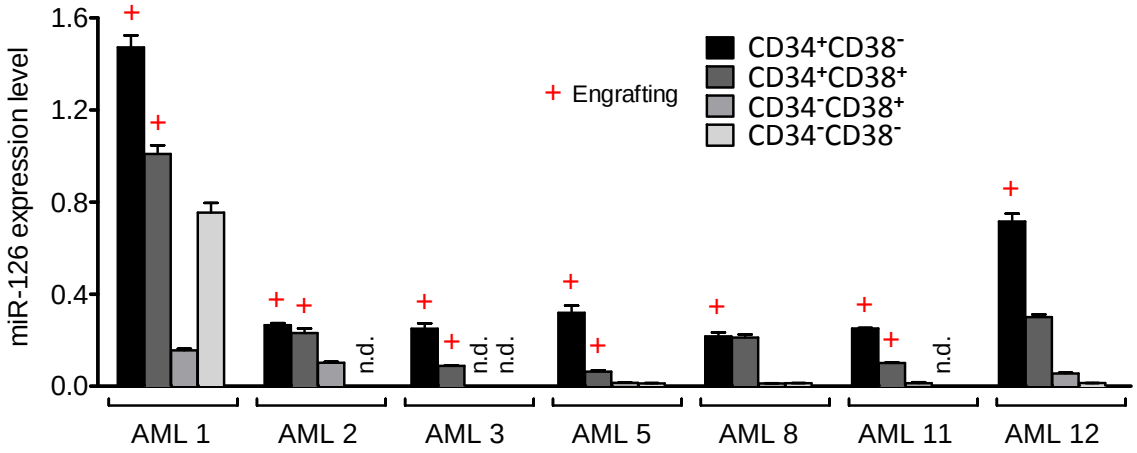

B

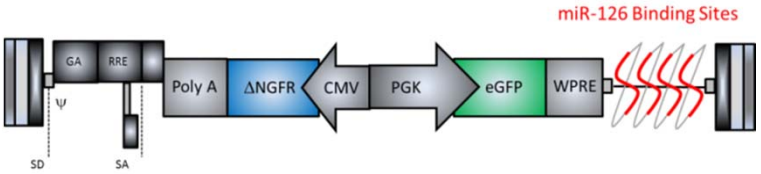

C

AML Sample	Population Gate	Fold miR-126 Enrichment from bulk	Fold miR-126 Enrichment from eGFP^{high}
AML 3	G6	0.08	1
	G5	3.2	43.1
	G4/G3	0.28	3.7
AML 7	G6	0.08	1
	G5	0.27	3.39
	G4/G3	3.39	42.3
AML 18	G6	0.02	1
	G5	1.16	45.4
	G4/G3	0.35	16

D

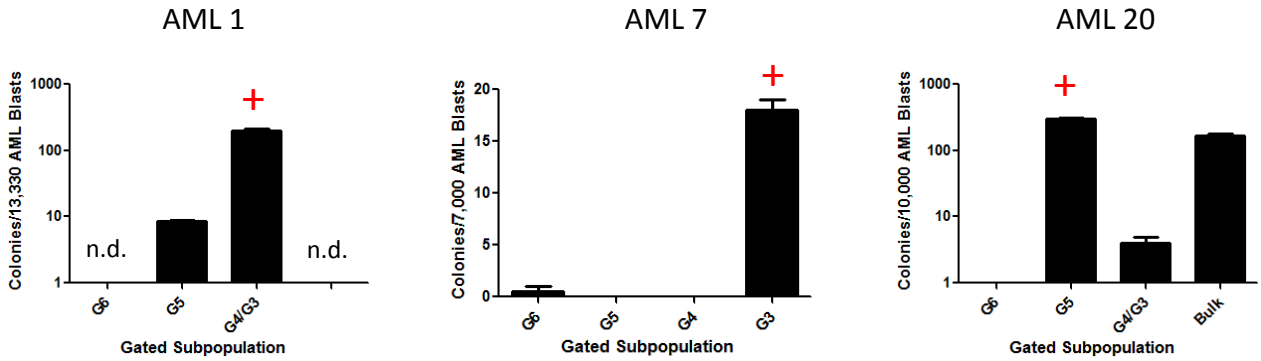

E

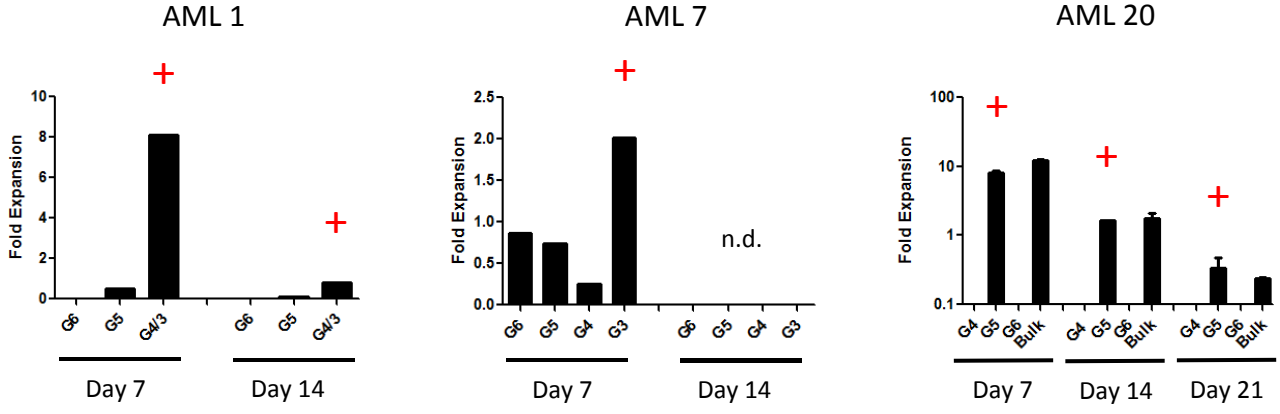

Figure S2, related to Figure 2. AML leukemia initiating capacity co-segregates with proliferation and clonogenic capacity of AML blasts.

(A) Quantitative PCR (qPCR) for mature miR-126 levels in flow sorted AML sub-fractions (see scheme depicted in **Figure 1A**). Data was normalized to RNU48 control levels. Results are shown as mean ± SEM of n=3 technical replicates.

(B) Schematic of the bi-directional miR-126 biosensor vector. The vector expresses truncated NGFR in one direction (which marks all transduced cells) and eGFP in the other direction. miR-126 binding sites are cloned downstream of eGFP. The more miR-126 a cell expresses, the less eGFP protein that is translated, leading to lower levels of eGFP fluorescence.

(C) Table depicting the normalized levels of mature miR-126-3p in biosensor sorted AML populations and measured by qPCR. In red text, the table shows the gated population most enriched in miR-126-3p levels compared to bulk AML or compared to $eGFP^{high}$ fractions (lowest miR-126 activity).

(D) Bar graphs representing the colony forming ability of flow sorted populations of miR-126 biosensor vector transduced primary AML patient samples after recovery from NSG mice. The red crosses indicate the gated populations that were able to recapitulate the AML ΔNGFR/eGFP hierarchy in vivo. Data represents mean ± SEM of n= 2 technical replicate experiments.

(E) Bar graphs showing proliferation capacity of flow sorted populations of miR-126 biosensor vector transduced primary AML patient samples after recovery from NSG mice. The red crosses indicate the gated populations that were able to recapitulate the AML ΔNGFR/eGFP hierarchy in vivo. Data represents mean ± SEM of n= 2 technical replicate experiments.

Table S2, related to Figure 2. AML Patient Samples Used for miR-126 Biosensor Lentivector in vivo Studies.

AML	Sample Type	FAB	Age	Sex	Karyotype	Engraftment of AML Subpopulations			
						$CD34^+$ $CD38^-$	$CD34^+$ $CD38^+$	$CD34^-$ $CD38^+$	$CD34^-$ $CD38^-$
1	Relapse	Unclass	48	F	46,XX,t(2;21)(p21;q22)[4]/46,XX,9(1;21)(q22;q22)	+	+	-	-
3	Diagnosis	Unclass	52	F	47,XX,+8	+	+	+	+
7	Diagnosis	Unclass	47.9	M	n.d.	+	-	-	+
18	Diagnosis	M4	34.8	M	45,XY, inv(3)(q21q26.2) -7[20]	NT	NT	NT	NT

(+) symbols at right represent CD34/CD38 fractions that engraft immuno-deficient mice. (-) symbols represent fractions that were functionally evaluated and do not engraft immuno-deficient mice. (NT) symbols represent fractions that were not evaluated for LSC activity.

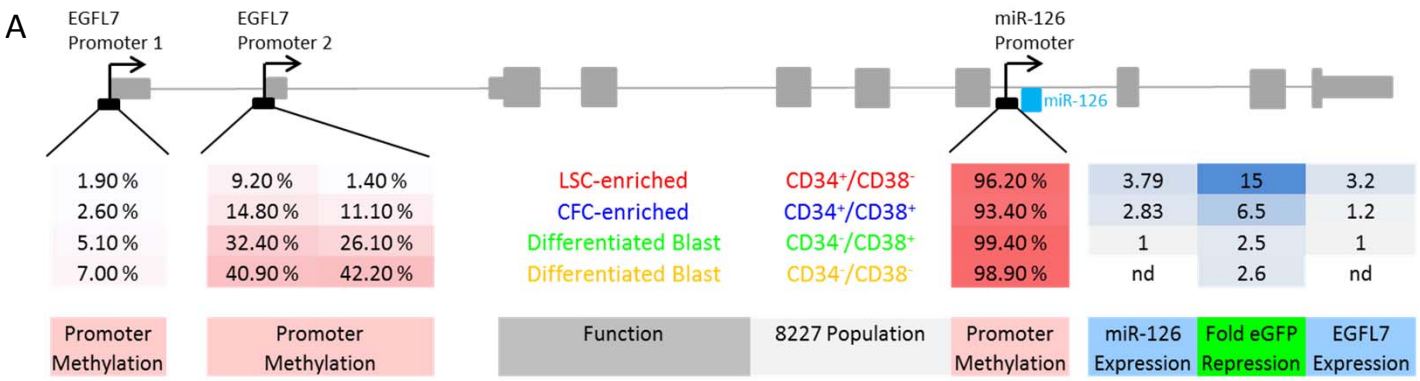
A
EGFL7 Promoter 1
EGFL7 Promoter 2
miR-126 Promoter
miR-126
1.90 %
2.60 %
5.10 %
7.00 %
9.20 %
14.80 %
32.40 %
40.90 %
1.40 %
11.10 %
26.10 %
42.20 %
LSC-enriched
CFC-enriched
Differentiated Blast
Differentiated Blast
CD34+/CD38-
CD34+/CD38+
CD34-/CD38+
CD34-/CD38-
96.20 %
93.40 %
99.40 %
98.90 %
3.79
2.83
1
nd
15
6.5
2.5
2.6
3.2
1.2
1
nd
Promoter Methylation
Promoter Methylation
Function
8227 Population
Promoter Methylation
miR-126 Expression
Fold eGFP Repression
EGFL7 Expression

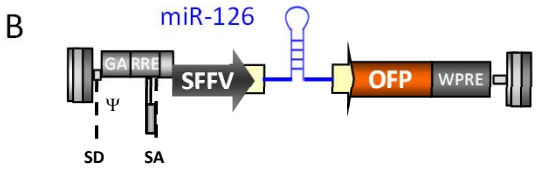
B
miR-126
GA
RRE
Ψ
SFFV
OFP
WPRE
SD
SA

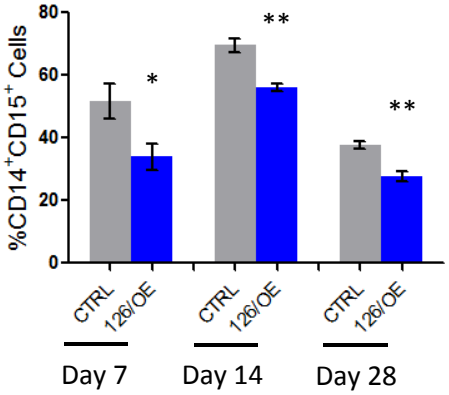
C
%CD14+CD15+ Cells
80
60
40
20
0
*
**
**
CTRL
126/OE
Day 7
Day 14
Day 28

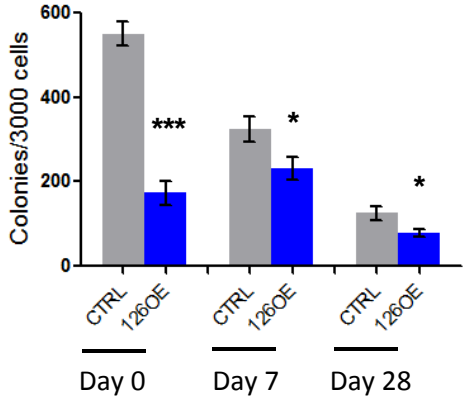
D
Colonies/3000 cells
600
400
200
0
***
*
*
CTRL
126OE
Day 0
Day 7
Day 28

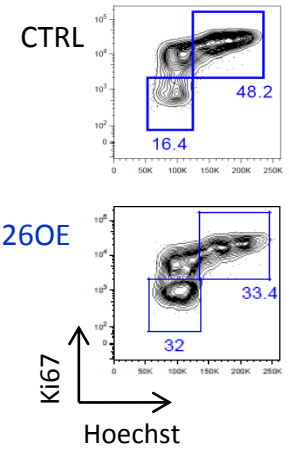
E
CTRL
48.2
16.4
126OE
33.4
32
Ki67
Hoechst

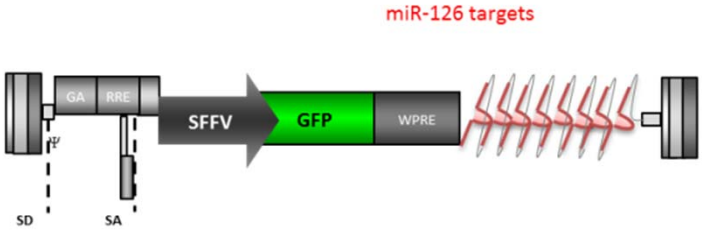
miR-126 targets
F
GA
RRE
Ψ
SFFV
GFP
WPRE
SD
SA

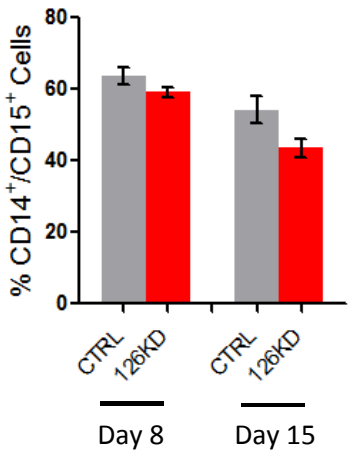
G
% CD14+/CD15+ Cells
80
60
40
20
0
CTRL
126KD
Day 8
Day 15

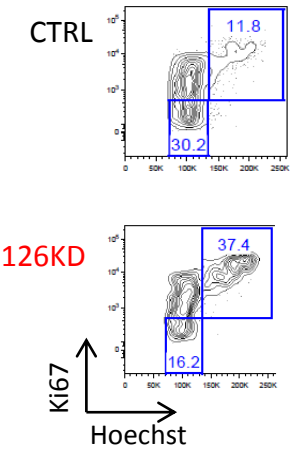
H
CTRL
11.8
30.2
126KD
37.4
16.2
Ki67
Hoechst

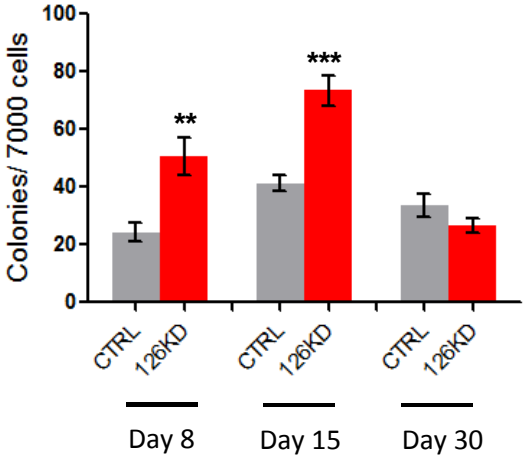
I
Colonies/ 7000 cells
100
80
60
40
20
0
**
***
CTRL
126KD
Day 8
Day 15
Day 30

Figure S3, related to Figure 3. Enforced expression and knockdown of miR-126 alters proliferation and differentiation status of primitive AML cells in vitro.

(A) Schematic of the EGFL7/miR-126 locus. Promoter methylation was determined by CD34/CD38 sorting of 8227 subpopulations. Methylated DNA immunoprecipitation (MeDIP) combined with tiling array hybridization. High methylation of the internal miR-126 promoter suggests that miR-126 expression is regulated from the EGFL7 promotor 2 site, which is progressively methylated with increasing differentiation of the 8227 cells. This differentiation is correlated with changes in cellular function as measured by in vitro culture initiation, in vivo leukemia initiation, colony forming capacity, and proliferation. Furthermore, miR-126 expression by array (normalized log2 transformed levels) and EGFL7 expression levels from array (normalized log2 transformed levels) are highest in the LSC enriched fraction and are progressively reduced with increasing differentiation. miR-126 bioactivity, as measured by the miR-126 biosensor vector, is highest in the LSC fraction and decreases with differentiation.

(B) Schematic representation of the lentiviral construct for enforced expression of miR-126. The human miR-126 hairpin is driven off of the SFFV promotor.

(C) 8227 leukemia cells were transduced with lentivectors expressing miR-126 (126OE) or an empty control vector (CTRL). Transduced cells were flow sorted for mOrange (mO^+) expression and plated in liquid culture conditions for 28 days with weekly passage. Graphical representation of the proportion of $CD14^+CD15^+$ in 8227 CTRL transduced cells or 126OE cells on days 7, 14 and 28 in post-sort cultures. Data represents mean $\pm$ SEM of n=3 replicate experiments where * $p < 0.05$, ** $p < 0.01$.

(D) Colony forming potential of CTRL and 126OE 8227 cells measured by methylcellulose CFC assay and evaluated a day 0, 7, and 28 of culture. Data represents mean $\pm$ SEM of n=2 technical replicate experiments where * $p < 0.05$, *** $p < 0.001$.

(E) Representative flow plots for cell cycle analysis with Hoechst and Ki67 cell staining of CTRL and 126/OE 8227 AML cells.

(F) Schematic representing the lentiviral sponge construct for knockdown of endogenous miR-126 activity. Eight imperfect miR-126 binding sites are cloned downstream of eGFP and driven off of an SFFV promotor.

(G) 8227 leukemia cells were transduced with lentivectors expressing miR-126 sponge (126KD) or an empty control vector (CTRL). Transduced cells were flow sorted for enhanced Green Fluorescent Protein ($eGFP^+$) expression and plated in liquid culture conditions for 30 days with weekly passage. Graph showing the proportion of $CD14^+CD15^+$ in 8227 CTRL transduced cells or 126KD cells at days 7 and 15 post-sort. Data represents mean $\pm$ SEM of n= 3 replicate experiments.

(H) Representative flow plots for cell cycle analysis with Hoechst and Ki67 cell staining of CTRL and 126KD 8227 AML cells.

(I) Graph showing colony forming potential of bulk miR-126KD 8227 cultures days 7, 15 and 30 after culture initiation. Data represents mean $\pm$ SEM of n= 3 replicate experiments where ** $p < 0.01$, *** $p < 0.001$.

A

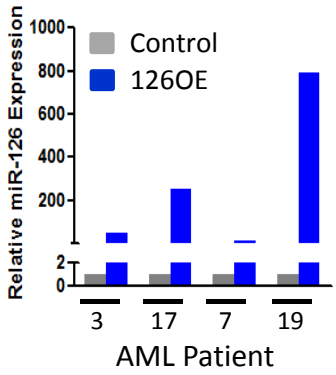

B

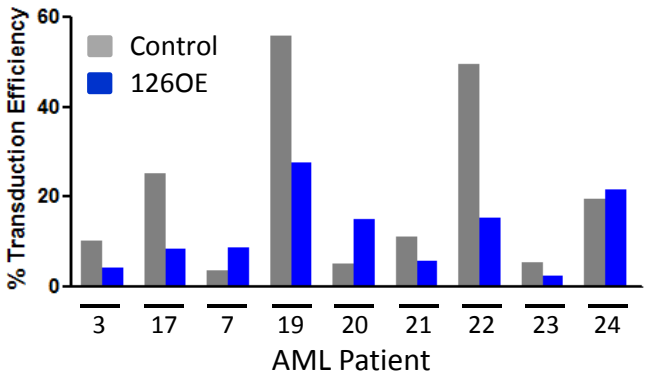

C

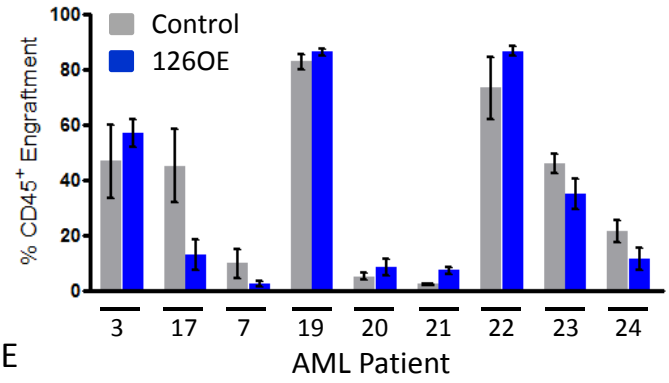

D

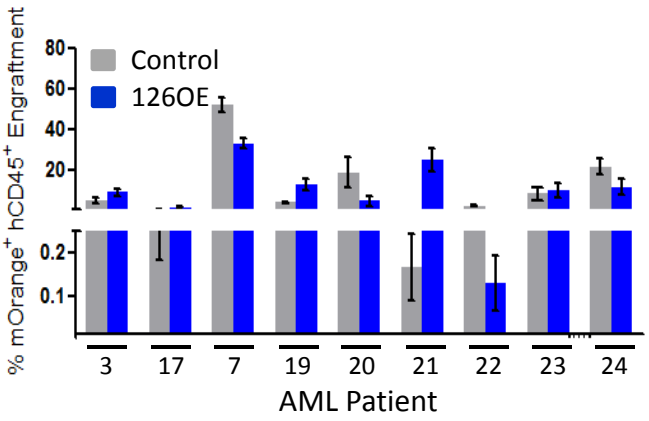

E

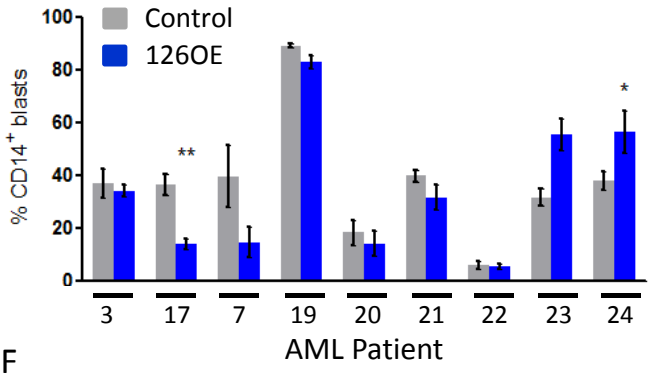

F

2° AML 3	# Cells Injected	% Mice Engrafted
CTRL	25,000	100% (2/2)
	5,000	0% (0/4)
	2,500	0% (0/5)
	500	0% (0/5)
126OE	25,000	100% (2/2)
	5,000	75% (3/4)
	2,500	0% (0/5)
	500	0% (0/5)

AML 17	# Cells Injected	% Mice Engrafted
CTRL	50,000	50% (1/2)
	25,000	0% (0/5)
	5,000	0% (0/5)
	1,000	0% (0/5)
126OE	50,000	100% (2/2)
	25,000	100% (5/5)
	5,000	80% (4/5)
	1,000	0% (0/5)

AML 7	# Cells Injected	% Mice Engrafted
CTRL	100,000	100% (2/2)
	25,000	20% (1/5)
	5,000	17% (1/6)
126OE	100,000	100% (4/4)
	25,000	100% (5/5)
	5,000	71% (5/7)

Group	Lower	Estimate	Upper
CTRL	103673	28175	7658
126OE	20845	8111	3156

Group	Lower	Estimate	Upper
CTRL	1587342	231601	33792
126OE	11021	4429	1780

Group	Lower	Estimate	Upper
CTRL	145005	52210	18799
126OE	9676	3942	1606

Figure S4, related to Figure 4. Increased miR-126 levels expand human AML LSC numbers in vivo.

(A) Relative levels of miR-126-3p expression for a subset of CTRL and 126/OE lentivirus transduced AML patient samples after 12 weeks in primary mice.

(B) Nine human AML samples were thawed, transduced overnight with lentiviruses expressing miR-126 (126/OE) or an empty vector (CTRL) and transplanted into NSG mice. After 12 weeks, mice were euthanized and bone marrow recovered for analysis. Percent AML cells transduced in 9 patient samples after overnight exposure to CTRL and 126/OE lentivirus (mOrange positivity) measured by flow cytometry 3 days post-virus transduction.

(C) Bar graph depicting changes in $hCD45^+$ levels within the bone marrow of transplanted mice after enforced expression of miR-126. Data shown represent the mean $\pm$ SEM of 4-6 mice

(D) Graphical representation of the proportion of mO^+hCD45^+cells in the bone marrow of CTRL and 126OE AML samples after 12 weeks. Data shown represent the mean $\pm$ SEM of 4-6 mice

(E) Graph of the proportion of $CD45^+mO^+CD14^+$ cells in the bone marrow of CTRL and 126OE AML samples after 12 weeks. Data shown represent the mean $\pm$ SEM of 4-6 mice where * $p < 0.05$, ** $p < 0.01$.

(F) Transduced human $CD45^+mO^+$ AML cells were flow sorted from primary mice and transplanted into secondary recipients for 8-10 weeks at limiting doses. Human $CD45^+$ marking > 0.5% was considered positive for AML engraftment. Human grafts were confirmed to be $CD33^+CD19^-$ AML. Tables depict transplanted cell numbers, engrafted mice percentages and numbers per CTRL and 126OE group for each AML patient sample.

Table S3, related to Figure 4. AML Patient Samples Used for in vivo Functional Evaluation of miR-126.

AML	Sample Type	FAB	Age	Sex	Karyotype	Engraftment of AML Subpopulations			
						$CD34^+$ $CD38^-$	$CD34^+$ $CD38^+$	$CD34^-$ $CD38^+$	$CD34^-$ $CD38^-$
17	Diag	Unclass	42.7	M	46, XY	+	+	+	+
19	Diag	Unclass	37.5	F	46,XX[18]: NPM1c+, FLT3-ITD+	+	+	-	+
20	Diag	M5a	60	M	45,X,-Y,t(11:19)(q23;p13.1)[20]	+	-	+	+
21	Diag	Unclass	31.5	F	46,XX,t(9;11)(p22;q23){[0]	NT	NT	NT	NT
22	Refractory	Unclass	36.7	M	46,XY,t(1;3)(q32;q26~27),del(20)(q13.1)[11]	NT	NT	NT	NT
23	Diag	M4	33.4	M	46,XY[20]; NPM1c+, FLT3-ITD+	NT	NT	NT	NT
24	Refractory	Unclass	70.7	F	46,XX,t(1;14)(q21;q11.2)[20]	NT	NT	NT	NT

(+) Symbols at right represent CD34/CD38 fractions that engraft immuno-deficient mice. (-) symbols represent fractions that were functionally evaluated by transplantation, but do not engraft immuno-deficient mice. (NT) symbols represent fractions that were not evaluated for LSC activity.

A

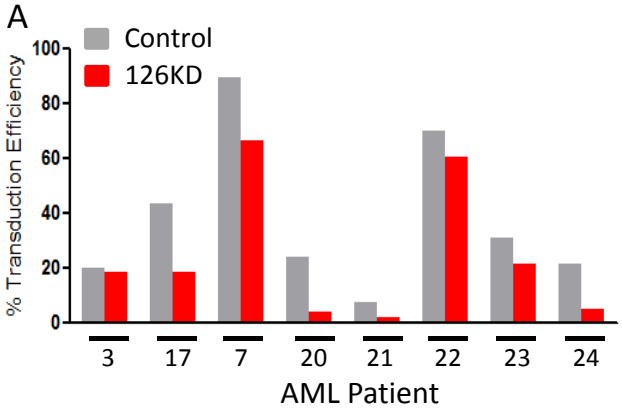

B

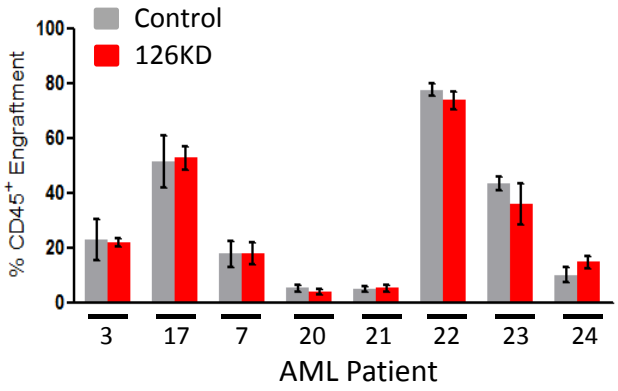

C

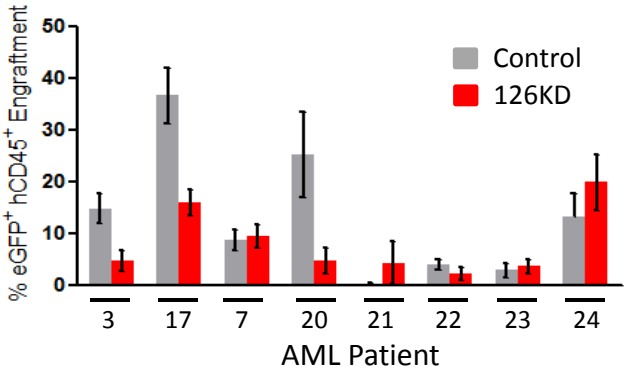

D

2°

AML 3	# Cells Injected	% Mice Engrafted
CTRL	625,000	100% (1/1)
	125,000	100% (5/5)
	25,000	100% (5/5)
	5,000	100% (4/4)
126KD	625,000	100% (2/2)
	125,000	100% (3/3)
	25,000	100% (5/5)
	5,000	0% (0/4)

Group	Lower	Estimate	Upper
CTRL	11524	3563	1102
126KD	31959	12615	4980

~3.47 Fold Decrease
In Frequency
p = 0.0087

AML 17	# Cells Injected	% Mice Engrafted
CTRL	300,000	100% (1/1)
	150,000	100% (4/4)
	75,000	100% (2/3)
126KD	300,000	100% (3/3)
	150,000	75% (3/4)
	75,000	0% (0/3)

Group	Lower	Estimate	Upper
CTRL	134514	49930	18533
126KD	197916	84804	36337

~1.7 Fold Decrease
In Frequency
p = 0.119

AML 7	# Cells Injected	% Mice Engrafted
CTRL	500,000	50% (2/1)
	250,000	100% (2/2)
	100,000	50% (2/4)
	25,000	0% (0/1)
126KD	500,000	50% (1/2)
	250,000	0% (0/1)
	100,000	75% (3/4)
	25,000	50% (1/2)

Group	Lower	Estimate	Upper
CTRL	646891	238740	88109
126KD	695315	239104	82223

No Fold Change
In Frequency
p = 0.998

Figure S5, related to Figure 5. Diminished miR-126 levels reduce the proportion of primitive AML cells

(A) Eight human AML samples were thawed, transduced overnight with lentiviruses expressing a miR-126 sponge (126KD) or an empty vector (CTRL) and transplanted into NSG mice. After 12 weeks, mice were euthanized and bone marrow recovered for analysis. Percent AML cells transduced in 8 patient samples after overnight exposure to CTRL and 126KD lentivirus (eGFP positivity) measured by flow cytometry 3 days post-virus transduction.

(B) Bar graph depicting changes in $hCD45^+$ levels within the bone marrow of transplanted mice with reduced expression of miR-126. Data shown represent the mean $\pm$ SEM of 4-6 mice.

(C) Proportional levels of $eGFP^+hCD45^+$cells in the bone marrow of CTRL and 126KD AML samples after 12 weeks. Data shown represent mean $\pm$ SEM of 4-6 mice.

(D) LSC frequency upon 126KD. Transduced human $CD45^+eGFP^+$ AML cells were flow sorted from primary mice and transplanted into secondary recipients for 8-10 weeks at limiting doses. Human $CD45^+$ marking >0.5% was considered positive for AML engraftment. Human grafts were confirmed to be $CD33^+CD19^-$ AML. Tables depict transplanted cell numbers, engrafted mice percentages and numbers per CTRL and 126KD group for each AML patient sample.

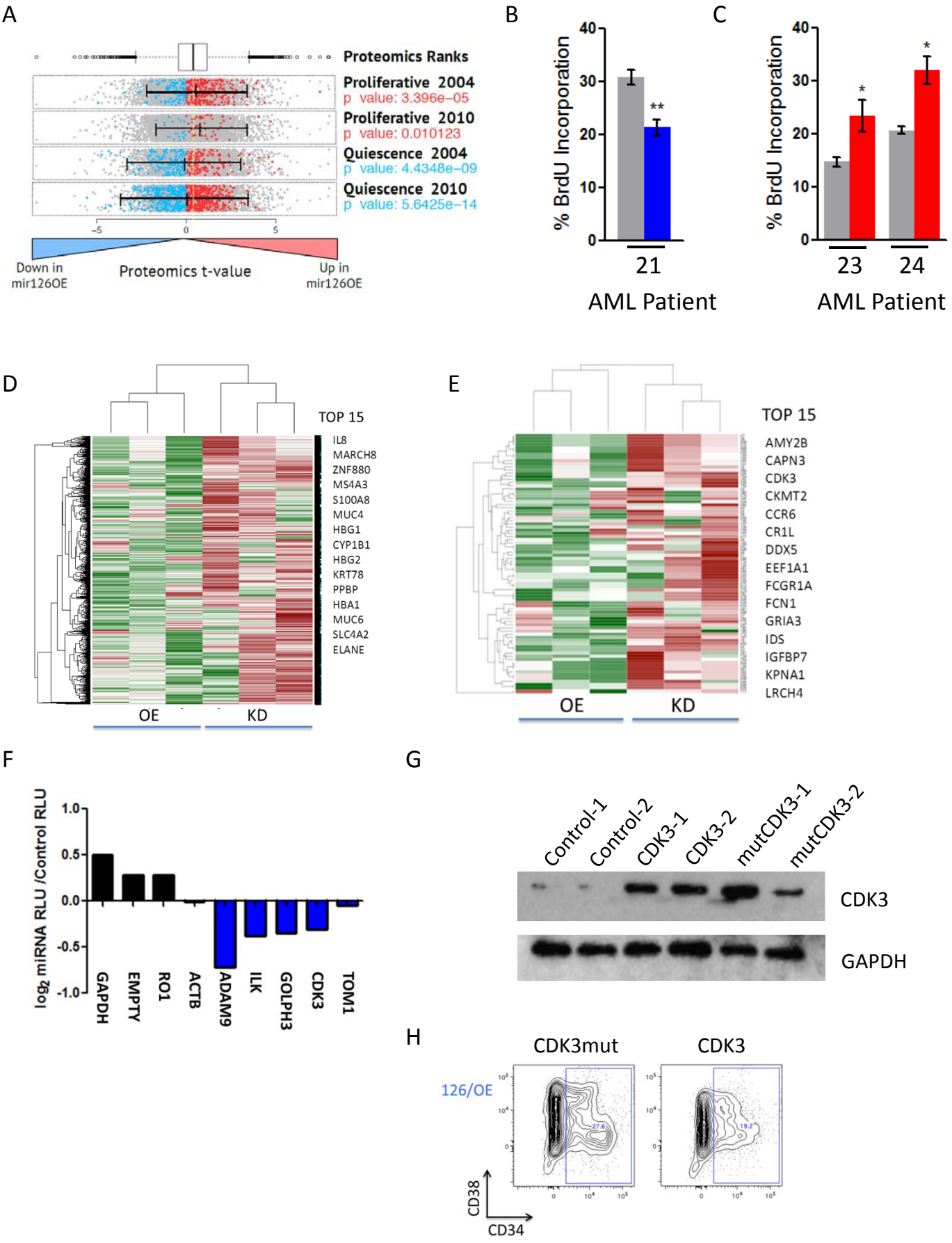
A
Proteomics Ranks
Proliferative 2004
p value: 3.396e−05
Proliferative 2010
p value: 0.010123
Quiescence 2004
p value: 4.4348e−09
Quiescence 2010
p value: 5.6425e−14
−5
0
5
Down in mir126OE
Proteomics t-value
Up in mir126OE
B
% BrdU Incorporation
40
30
20
10
0
**
21
AML Patient
C
% BrdU Incorporation
40
30
20
10
0
*
*
23
24
AML Patient
D
TOP 15
IL8
MARCH8
ZNF880
MS4A3
S100A8
MUC4
HBG1
CYP1B1
HBG2
KRT78
PPBP
HBA1
MUC6
SLC4A2
ELANE
OE
KD
E
TOP 15
AMY2B
CAPN3
CDK3
CKMT2
CCR6
CR1L
DDX5
EEF1A1
FCGR1A
FCN1
GRIA3
IDS
IGFBP7
KPNA1
LRCH4
OE
KD
F
log2 miRNA RLU /Control RLU
1.0
0.5
0.0
-0.5
-1.0
GAPDH
EMPTY
RO1
ACTB
ADAM9
ILK
GOLPH3
CDK3
TOM1
G
Control-1
Control-2
CDK3-1
CDK3-2
mutCDK3-1
mutCDK3-2
CDK3
GAPDH
H
CDK3mut
CDK3
126/OE
27.6
19.2
CD38
CD34

Figure S6, related to Figure 6. miR-126 targets CDK3 in primitive AML cells and enforced expression can rescue the 126OE phenotype in vitro

(A) Comparison of the proteomics data against published quiescent/proliferative signatures. For the proliferative gene sets, Mann Whitney non-parametric analysis was used to test the significance of the overlap between the published proliferative signatures and the proteomic gene set that was up-regulated in miR-126OE. For the quiescent gene sets, Mann Whitney non-parametric analysis was used to look for significance of the overlap between the quiescent signature and proteomic gene set that was down-regulated in miR-126OE. Grey dots represent all the different proteomics ranks t values. Red dots represent proteins found in the gene set of interest with a t-value greater than 0. Blue dots represent proteins found in the gene set of interest with a t value less than 0. The p value indicated below each gene set is the most significant Wilcox p value from the two scenarios tested, "greater" (red), "less" (blue). The yellow dotted line shows the mean of the proteomic ranks t-values.

(B) Human AML samples were thawed, transduced overnight with lentiviruses expressing miR-126 (126OE), a miR-126 sponge (126KD) or an empty vector (CTRL) and transplanted into NSG mice for 8-12 weeks. Sixteen hours prior to mouse euthanization, 1 mg BrdU in 200µl of sterile PBS was IP injected into each mouse. Bone marrow was recovered and processed for analysis. Graph showing proliferation measured by BrdU incorporation assay of CTRL or 126OE transduced AML cells in vivo. Data is shown as mean ± SEM of 5 replicate animals where ** $p<0.01$.

(C) Proliferation measured by BrdU incorporation assay of CTRL or 126KD transduced AML cells in vivo. Data is shown as mean ± SEM of 5 replicate animals where * $p<0.05$.

(D) Heat map ranking all genes that significantly increased in expression with miR-126KD and decreased in expression after miR-126OE in primitive 8227 AML cells. Green indicates decreased expression, red indicates increased expression upon miR-126 modulation. Columns indicate three replicate experiments.

(E) Heatmap of 84 miR-126 predicted targets listed in descending order of level of increase after 126KD. Green indicates decreased expression, red indicates increased expression upon miR-126 modulation. Columns indicate three replicate experiments. Note that CDK3 is near the top of listed targets.

(F) Validation of miR-126 predicted targets by luciferase 3' UTR reporter assay.

(G) Construction and functional validation of CDK3OE and control CDK3mutOE (kinase mutant) vectors. Western blot analysis shows high expression of CDK3 and mutCDK3 7 days post transduction of 8227 cells.

(H) CDK3OE rescue of $CD34^+$ cell expansion upon 126OE. The percentage of $CD34^+$ cells in double transduced cultures is shown as representative flow plots.

Table S4, related to Figure 6. Table S4 is provided as an Excel file

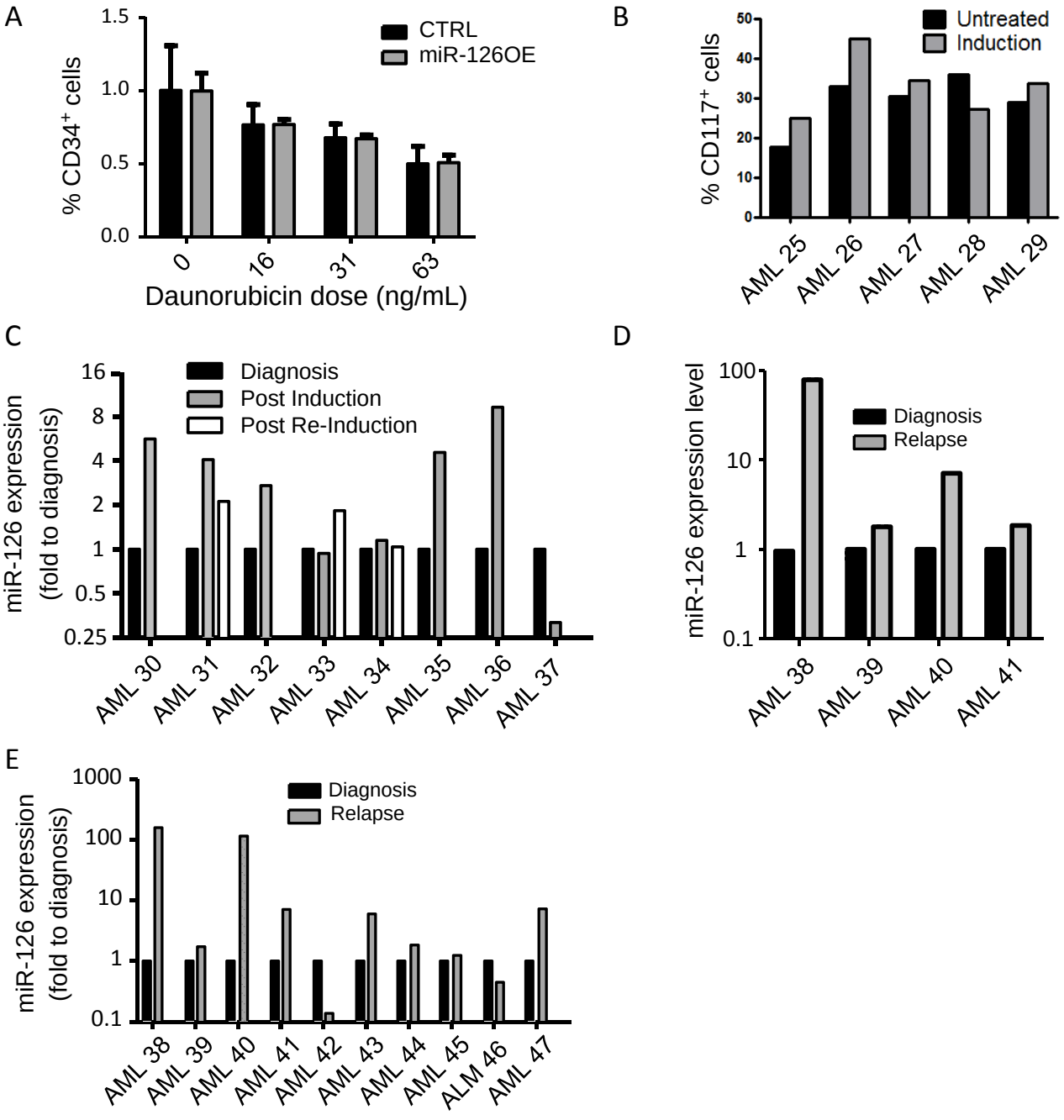
A
% CD34+ cells
1.5
1.0
0.5
0.0
CTRL
miR-126OE
0
16
31
63
Daunorubicin dose (ng/mL)
B
% CD117+ cells
50
40
30
20
10
0
Untreated
Induction
AML 25
AML 26
AML 27
AML 28
AML 29
C
miR-126 expression
(fold to diagnosis)
16
8
4
2
1
0.5
0.25
Diagnosis
Post Induction
Post Re-Induction
AML 30
AML 31
AML 32
AML 33
AML 34
AML 35
AML 36
AML 37
D
miR-126 expression level
100
10
1
0.1
Diagnosis
Relapse
AML 38
AML 39
AML 40
AML 41
E
miR-126 expression
(fold to diagnosis)
1000
100
10
1
0.1
Diagnosis
Relapse
AML 38
AML 39
AML 40
AML 41
AML 42
AML 43
AML 44
AML 45
ALM 46
AML 47

Figure S7, related to Figure 7. High expression of miR-126 protects primitive AML cells from chemotherapy and is a biomarker of refractory LSC.

(A) Graphical representation of non-transduced $CD34^+$ 8227 cells with increasing doses of Daunorubicin. Bars represent mean ± SEM of 3 independent cultures with 10 replicate wells each.

(B) Primary patient AML cells were plated onto MS5 stroma, after 24 hours cells were treated with vehicle or with Daunorubicin/AraC for 72 hours. Cells were recovered and evaluated for live cell content and immuno-phenotype by flow cytometry. Graphical representation of flow cytometry results of chemotherapy treated AML stromal cultures shows an increase in $CD117^+$ AML blasts after 72 hour treatment with Daunorubicin/AraC.

(C) miR-126 levels in 8 individual AML patients who failed to achieve complete remission (CR) after anthracycline/cytarabin induction chemotherapy. qPCR was performed on $CD45^{dim}$ sorted blasts from 8 patient samples at diagnosis (n=8, day 0) and, at day 14 (n=4) and day 30 (n=5) after initiation of induction chemotherapy, as well as on day 30 after (unsuccessful) salvage chemotherapy (n=3).

(D-E) Levels of miR-126 in individual paired diagnosis/relapse AML patient samples. AML patient samples were thawed and sorted for $CD45^{dim}$ or $CD45^{dim}CD117^+$ or $CD45^{dim}CD34^+$ populations. qPCR was used to evaluate the relative levels of miR-126 in paired patient samples. Graphical representation of miR-126 levels in $CD45^{dim}$ (D) and $CD45^{dim}CD117^+$ (samples 38-45) and $CD45^{dim}CD34^+$ (samples 46-47) (E) AML blasts in paired diagnosis/relapse samples.

Table S5, related to Figure 7. Clinical and Molecular Characteristics of AML Patients

AML	Age	Sex	De novo/Secondary	FAB	WBC	Cytogenetics	NPM1 mutation status	FLT3-ITD mutation status
AML Samples used in Stromal Assay								
25	72	M	sAML	n.d.	43	45,X,-Y[20]	n.d.	n.d.
26	28	F	de novo	M1	105.8	46,XX[20]	(+)	(-)
27	58	F	de novo	M5	35.6	46,XX[20]	(+)	(+)
28	50	M	de novo	M4Eo	41.3	46, XY, inv(16)(p13.1q22)[17]/47,idem,+22[3]	n.d.	n.d.
29	67	F	de novo	M1	128	46,XX[20]	n.d.	n.d.
Diagnosis/Refractory AML Patient Sample Pairs								
30	72	M	de novo	M2	41.8	46,XY T(10;13)(q24;q22)[20]	(+)	(+)
31	67	M	sAML	M4Eo	3.7	46,XY[20]	(+)	(-)
32	72	M	de novo	M5B	6.1	Complex/Pseudodiploid	(-)	(-)
33	48	M	de novo	M2	5	46,XY[20]	(-)	(-)
34	42	M	sAML	M2	2.4	Complex	(-)	(-)
35	50	M	de novo	M1	116.9	46,XY[20]	(+)	(+)
36	68	M	de novo	M2	2.1	46,XY[20]	(+)	(-)
37	37	F	de novo	M2	60	46,XX[20]	(+)	(+)
Diagnosis/Relapse AML Patient Sample Pairs								
38	75	M	de novo	M1	60	46,XY[20]	(+)	(-)
39	43	M	de novo	M4Eo	55	46,XY[20]	(+)	(-)
40	60	M	de novo	M4Eo	108	46,XY[20]	(+)	(-)
41	60	M	sAML	M5a	134	45,X,-Y,t(11;19)(q23;p13.1)[20]	n.d.	n.d.
42	27	F	de novo	M2	150	n.d.	(-)	(-)
43	77	M	de novo	M2/M4	215	n.d.	(-)	(+)
44	77	M	de novo	M5	73.9	46,XY[20]	(+)	(+)
45	49	F	de novo	M2	n.d.	46,XX, t(8;11)(q24.2-3;q1)[20]	(+)	(+)
46	72	F	de novo	M4	11.6	46,XX[20]	(-)	(-)
47	52	F	de novo	M4	56.7	46,XX[20]	(-)	(-)

Clinical parameters of the AML patient bone marrow samples used for in vitro stromal chemotherapy assay (AML 19 to AML 23), AML patient cohort that failed to achieve complete remission (AML 24 to AML 31), and paired diagnosis/relapse AML patient samples (AML32 to AML 41).

SUPPLEMENTAL EXPERIMENTAL PROCEDURES

Limiting dilution analysis

$CD45^+mO^+$ (miR-126OE) or $CD45^+eGFP^+$ (miR-126KD) cells from pooled bone marrow (BM) of primary mice 12 weeks after transplantation and injection of various cell doses into conditioned secondary recipients. A secondary mouse was scored as positive if it had >0.5% BM engraftment 12 weeks after transplantation. Leukemia stem cell (LSC) frequency was estimated by linear regression analysis and Poisson statistics using publicly available ELDA (Extreme Limiting Dilution Analysis, http://bioinf.wehi.edu.au/software/elda/) software (Hu and Smyth, 2009).

Nanostring miRNA data generation and processing

The expression of 30 miRNAs from 74 acute myeloid leukemia (AML) samples from Princess Margaret Cancer Centre (PMCC) were measured and normalized using the NanoString platform (Geiss et al., 2008). For the TCGA cohort, miRNA-Seq RPM (i.e., reads per million) normalized profiles generated using the Illumina Genome Analyzer, which captured the expression of ~492 miRNAs, were downloaded from the TCGA data portal (Cancer Genome Atlas Research Network, 2013). The maximum linear expression of 29 mature miRNAs that were common to both datasets was analyzed in this study. All miRNA expression values were increased by one plus a small normally distributed random value to produce non-zero expression profiles. These profiles were then $\log_2$ transformed and filtered for miRNAs with high variance (i.e., values outside of the 20^{th} to 80^{th} percentile range). Finally, ComBat normalization was applied to reduce the cross-platform differences (i.e., batch effects) between the 2 datasets (Johnson et al.,

2007)(Fei et al., 2013)(Rudy and Valafar, 2011)(Sirinukunwattana et al., 2013). All data analysis was done in R 2.15.2.

Building prognostic miRNA signatures

The glmnet 1.9-3 R package was configured for L1 regularized Cox regression, enabled with leave one out cross validation. This statistical learning tool was then applied to the PMCC dataset to select a minimal weighted combination of miRNA expression that best explained patient survival time. This training phase resulted in a 4-miRNA signature that was tested for prognostic value in the TCGA dataset. Per-patient risk scores were computed using dot products between the expression of signature miRNAs (i.e., c_i) and their corresponding regression coefficients (i.e., weights w_i) as follows: $(w_1 \times c_1) + (w_2 \times c_2) + (w_3 \times c_3) + \ldots$ etc. The resulting continuous scores were further discretized based on the 50th percentile (i.e., median) split, where patients with scores above the split were considered to be at high risk (else low risk) as previously described (Eppert et al., 2011).

miRNA signature performance

In survival analysis, overall survival (OS) was defined as the time from AML diagnosis until death from any cause, event-free survival (EFS) was defined as the time from AML diagnosis until induction failure, relapse, or death from any cause, and relapse-free survival (RFS) defined as the time from the date of first complete remission (CR1) until relapse or death, regardless of cause (Cheson et al., 2003). The survival 2.37-4 package in R (Borgan, 2001) was used to assess the prognostic value of the miRNA signature scores computed for each patient in the TCGA dataset. Survival differences between patients with low- and high- signature scores were assessed using uni- and multi- variate Cox proportional hazards (CPH) and Kaplan-Meier models. In the multivariate case, the prognostic impact of white blood count (WBC), gene mutational status

(i.e., *NPM1*, *FLT3*ITD), age, type of AML onset (i.e., de-novo, secondary), and cytogenetic risk group (i.e., favorable, intermediate, or adverse) served as controls based on their established prognostic relevance in AML and patient data availability (Cancer Genome Atlas Research Network, 2013)(Eppert et al., 2011). The proportional hazards assumption was tested by examining Schoenfeld residuals for each patient parameter (e.g., WBC, age) used in the survival models. Parameters that significantly ($p<0.05$) violated this assumption were used to construct a stratified CPH model to remove their non-proportionality effects on hazard. Signature performance was assessed based on: (1) the lower 95% confidence interval of the signature scores' hazard ratio being greater than the value of one in multivariate survival analysis ($p< 0.05$, Wald test); and (2) the ability of the signature scores to significantly dichotomize low- from high- risk patients in univariate survival models ($p<0.05$, log rank test).

Illumina Microarray

8227 cells were transduced with miR-126/OE or miR-126/KD vectors or their respective empty control lenti-vectors at a multiplicity of infection (MOI) of 30. Cells were expanded under standard culture conditions for two weeks post-transduction and then flow sorted into $CD34^{+}CD38^{-}$, $CD34^{+}CD38^{+}$ and $CD34^{-}CD38^{+}$ populations. Recovered cells were stored in Trizol (Invitrogen) at -80^{o}C. RNA from transduced 8227 cells was extracted using Trizol (Invitrogen) and gene expression assayed on HT-12_v4 microarrays (Illumina). Quantile normalization was performed and probes were filtered by detection p-value (<0.1) (GeneSpring GX, Agilent). Next, to remove uninformative probes, those that did not exceed a threshold of 7.8 in all replicates of any one condition were eliminated, leaving 15812 probes for analysis.

Gene set enrichment analysis

Gene set enrichment analysis was performed using g:Profiler software with the options significant only, ordered query on 2564 genes selected based both on a positive log fold change (logFC) in 8227 126/KD and a negative logFC in 8227 126/OE versus Control samples (Reimand et al., 2011). Gene-sets with a size equal or greater than 500 were removed. Results were visualized using Cytoscape 2.8.1 (Smoot et al., 2011) and an enrichment map (version 1.2 of Enrichment Map software (Merico et al., 2010) was generated using enriched gene-sets with a p-value <0.05 and overlap coefficient set of 0.5.

Mass Spectrometry Sample Preparation

One to two weeks post viral transduction, 8227 cells with miR-126 overexpression (126/OE) and control vector (CTRL) were counted and washed twice with ice-cold PBS. 100,000 cells for each experimental condition, in biological triplicate, were subjected to sample preparation similar to (Kulak et al., 2014). Cells were lysed using 50 µl of lysis buffer (consisting of 6 M Guanidinium Hydrochloride, 10 mM TCEP, 40 mM CAA, 100 mM Tris pH8.5). Samples were boiled at 95^{o}C for 5 minutes, after which they were sonicated on high for 3x 10 seconds in a Bioruptor sonication water bath (Diagenode) at 4^{o}C. Samples were diluted 1:3 with 10% Acetonitrile, 25 mM Tris pH 8.5, LysC (MS grade, Wako) was added in a 1:50 (enzyme to protein) ratio, and samples were incubated at 37^{o}C for 4hrs. Samples were further diluted to 1:10 with 10% Acetonitrile, 25 mM Tris pH 8.5, trypsin (MS grade, Promega) was added in a 1:100 (enzyme to protein) ratio and samples were incubated overnight at 37^{o}C. Enzyme activity was quenched by adding 2% trifluoroacetic acid (TFA) to a final concentration of 1%. Prior to mass spectrometry analysis, the peptides were fractionated using Strong Cation Exchange (SCX) in StageTip format. For each sample, 6 discs of SCX material (3M Empore) were packed in a 200ul tip, and the SCX material activated with 80 µl of 100% Acetonitrile (HPLC grade, Sigma). The tips were

equilibrated with 80 µl of 0.2% TFA, after which the samples were loaded using centrifugation at 4,000x rpm. After washing the tips twice with 100µl of 0.2% TFA, five initial fractions were eluted into clean 500µl Eppendorf tubes using 50, 75, 125, 200 and 300mM ammonium acetate, 20% Acetonitrile, 0.5% formic acid respectively. The final fraction was eluted using 5% ammonium hydroxide, 80% Acetonitrile. The eluted fractions were frozen on dry ice and concentrated in an Eppendorf Speedvac, and re-constituted in 1% TFA, 2% Acetonitrile for Mass Spectrometry (MS) analysis.

Mass Spectrometry Acquisition

For each SCX fraction, peptides were loaded onto a 50cm C18 reverse-phase analytical column (Thermo EasySpray ES803) using 100% Buffer A (0.1% Formic acid in water) at 750bar, using the Thermo EasyLC 1000 µHPLC system in a single-column setup and the column oven operating at 45°C. Peptides were eluted over a 140 minute gradient ranging from 5 to 48% of 100% acetonitrile, 0.1% formic acid at 250 nl/min, and the Orbitrap Fusion (Thermo Fisher Scientific) was run in a 3 second MS-OT, ddMS2-IT-HCD top speed method. Full MS spectra were collected at a resolution of 120,000, with an AGC target of 4×10^5 or maximum injection time of 50ms and a scan range of 400–1500m/z. Ions were isolated in a 1.6m/z window, with an AGC target of 1×10^4 or maximum injection time of 50ms, fragmented with a normalized collision energy of 30 and the resulting MS2 spectra were obtained in the ion trap. Dynamic exclusion was set to 60 seconds, and ions with a charge state <2, >7 or unknown were excluded. MS performance was verified for consistency by running complex cell lysate quality control standards, and chromatography was monitored to check for reproducibility. Each sample was run in technical duplicate and biological triplicate, and the reproducibility of the analyses is depicted in **Table S4**. The mass spectrometry data have been deposited to the ProteomeXchange

Consortium (http://proteomecentral.proteomexchange.org) via the PRIDE partner repository with the dataset identifier PXD001994 (username: reviewer02600@ebi.ac.uk, password: aLahIn44)(Hermjakob and Apweiler, 2006).

Label-free Quantitative Proteomics Analysis

The raw files were analyzed using MaxQuant version 1.5.2.8 (Cox and Mann, 2008) and standard settings. Briefly, label-free quantitation (LFQ) was enabled with a requirement of 3 unique peptides per protein. Variable modifications were set as Oxidation (M), Acetyl (protein N-term), Gln->pyro-Glu and Glu->pyro-Glu. Fixed modifications were set as Carbamidomethyl (C), false discovery rate was set to 1% and "match between runs" was enabled. The resulting protein groups file, containing all the LFQ intensities across all the samples was processed in Perseus (filtering for contaminants and reverse hits), resulting in 8,848 proteins identified in total, and 4,837 proteins quantified across all samples. To determine those proteins that are significantly different between 126OE and CTRL samples, the ratios of 126OE vs CTRL were calculated in each biological repeat and subjected to statistical analysis in Limma (R Statistical Framework) with Benjamini-Hochberg adjustment. This table is included as **Table S4**, and was used as input for downstream analysis with GSEA.

Proteomics

MaxQuant LFQ (Cox and Mann, 2008) intensities were used as a measure of protein expression in 8227 126OE and control samples. The entire protein expression set consisting of 3 biological replicates for each treatment group and corresponding technical replicates (total of 12 samples) was quantile normalized in R (R version 3.1.1) using the normalizer package (version 1.0). The normalized protein expression was further filtered to contain only proteins that had at least two measurements in either treatment or control.

Difference in protein expression between the groups was assessed using a moderated t-test available in the bioconductor limma package (version 3.20.9). P-values were further corrected to control for multiple hypothesis testing using the Benjamini-Hochberg procedure. 638 proteins had significant differential expression with nominal p-value <0.05, of those 451 were upregulated (t>0) and 187 were downregulated (t<0). Proteins and their corresponding t-statistic were used to create a rank file to be used in pathway analysis described below.

Pathway Analysis on the proteomics data

Gene Set Enrichment Analysis (Subramanian et al., 2005) was performed using the protein expression ordered from largest to smallest t statistics with parameters set to 1000 gene-set permutations and gene-sets size between 5 and 500. The gene-sets included for the GSEA analyses were obtained from KEGG, MsigDB-c2, NCI, Biocarta, IOB, Netpath, HumanCyc, Reactome, Panther and Gene Ontology (GO) databases, updated December 24, 2014 (http://download.baderlab.org/EM_Genesets/). An enrichment map (version 2.1.0 of Enrichment Map software (Merico et al., 2010) was generated using Cytoscape 3.2.1 using significantly enriched gene-sets with a nominal p-value <0.05 and FDR <0.01. Similarity between gene-sets was filtered by Jaccard coefficient >0.25. Only gene-sets enriched in downregulated proteins were further analyzed and visualized.

Correlation between miR-126 predicted targets and the proteomics modulated pathway

Four databases were used to create a list of miR-126 predicted targets (DIANA microT, picTar, TargetScan from the miRbase website (http://www.mirbase.org)) and miRanda from the microCosm website (http://www.ebi.ac.uk/enright-srv/microcosm/htdocs/targets/v5/). Downregulated predicted targets were compared to enriched gene-sets in the enrichment map and significance of overlap was scored using 2 statistical tests (a hypergeometric test and a one-

sample Wilcoxon rank sum test) so that highest significance corresponds to higher number of genes in each overlap relative to gene-set size (hypergeometric test) and proteins in the overlap showing the highest differential expression amplitude (one sample Wilcoxon test).

Correlation between the transcriptomic data and the proteomic modulated pathways

2564 genes were selected based both on a positive log fold change (logFC) in 8227 126KD and a negative logFC in 8227 126OE versus control samples. The list was ranked by the 8227 126KD logFC in a decreasing order and compared to enriched gene-sets in the enrichment map and significance of overlap was scored using 3 statistical tests (one hypergeometric test, two one-sample Wilcoxon rank sum tests) so that highest significance corresponds to a higher number of genes in each overlap relative to gene-set size (Hypergeometric test), genes in the overlap showing higher differential expression amplitude (one sample Wilcoxon test), and proteins in the overlap showing higher differential expression amplitude (one sample Wilcoxon test).

Correlation of the miR-126 predicted targets and the miR-126 modulated pathways

Four databases were used to create a list of miR-126 predicted targets (DIANA microT, picTar, TargetScan from the miRbase website (http://www.mirbase.org)) and miRanda from the microCosm website (http://www.ebi.ac.uk/enright srv/microcosm/htdocs/targets/v5/). 84 predicted targets were part of the 2564 genes up-regulated in 8227 126KD and down-regulated in 8227 126OE. This list was compared to enriched gene-sets in the enrichment map and overlap was scored using Fisher's Exact Test p-value. Overlaps with p-value <0.05 were visualized.

Global miRNA Profiling

As described in (Eppert et al., 2011), cells from 16 AML patients (**Figure S1A**) were stained with antibodies to cell surface markers CD34 and CD38 and flow sorted into $CD34^{+}CD38^{-}$,

$CD34^+CD38^+$, $CD34^-CD38^+$ and $CD34^-CD38^-$ populations. Three independent pooled cord blood samples from 15–22 donors were used for isolation of HSC subsets and progenitors. Representative sorting gates are in **Figure 1A**.

NSG mice 8–13 weeks old were pretreated with 2.75–3.4 Gy radiation before being injected intra-femorally with AML cells at a dose of 200 to 2.87×10^6 sorted cells per mouse, as described (Eppert et al., 2011). Mice were killed at 12 weeks (mean 10 weeks), and bone marrow from the injected right femur, opposite femur and, in some cases, both tibias and spleen were collected for flow cytometry and secondary transplantation. Human engraftment was evaluated by flow cytometry of the injected right femur and non-injected bones and spleen. A threshold of 0.5% human $CD45^+$ cells in bone marrow was used as positive for human engraftment. Secondary transplantation was done by intrafemoral injection of cells from either right femur or pooled bone marrow from primary mice into one to three secondary mice pretreated with irradiation and antibody to CD122.

miRNA labeling

Target preparation was done according to (Lu et al., 2005). Briefly, two synthetic pre-labeled control nucleotides (5' – pCAGUCAGUCAGUCAGUCAGUCAG-3', and 5'-pGACCUCCAUGUAACGUACAA-3', Dharmacon) were spiked at 3fmoles per μg of total RNA to control for target preparation control. Small RNA's were recovered for 1-10 μg total RNA by PAGE purification and adaptor ligated sequentially on the 3' end and the 5' end using T4 RNA ligase (Amersham Biosciences). After reverse transcription using adaptor specific primers, products were PCR amplified for 18 cycles for 10 μg starting total RNA using 3' – primer 5'-TACTGGAATTCGCGGTTA-3' and 5' primer-biotin-CAAACGAATTCCTCACTAA-3'(IDT). PCR products were precipitated and dissolved in 66

μl TE buffer (10 mM Tris-HCL pH 8.0, 1 mM EDTA) containing two biotinylated post-labelling control oligonucleotides (100 fmoles of FVR506, 25 fmoles PTG20210).

Bead based detection

As described in (Lu et al., 2005), miRNA capture probes were conjugated to carboxylated xMAP beads (Luminex Corportion) in a 96-well plate. Samples were hybridized in a 96 well plate, with 2 mock PCR samples in each plate as a background control. Hybridization was carried out overnight. Beads were spun down, resuspended in 1x TMAC containing 10 $\mu g/mL^{-1}$ streptavividin-phycoerythrin (Molecular probes) before data acquisition of a Luminex 1001S machine. Median fluorescence intensity values were measured.

miRNA array computational analysis

Profiling data was scaled to the post-labelling controls and then the pre-labelling controls, in order to normalize readings from different probe/bead sets for the same sample and to normalize for the labelling efficiency, respectively. Data were threshholded at 32 and $\log_2$ transformed. The LSC miRNA signature was generated using a Smyth's moderated t-test with Benjamini-Hochberg multiple testing correction to compare fractions positive for LSCs versus those without LSCs.

Luciferase Reporter assay

Luciferase assay (Switchgear Genomics) was performed according to the manufacturers' protocol. Briefly, 293T cells were seeded to 40% confluency in 100 μl total volume in 96 well white TC plates (NUNC). The next day, equal volumes of mixture 1 (GoClone reporters; 30 ng/μl, miR-126 mimic or non-targeting mimic; 100 nM, and serum free media) was combined with mixture 2, (Dharmafect Duo/serum-free media) and incubated at room temperature RT for

20 minutes. After incubation, 4 volumes of pre-warmed serum-free media were added and mixed. 100 μl of the mixture was added to each well containing 293T cells and incubated overnight. Reconstituted luciferase substrate (100 μl) was added to each well, incubated at RT for 30 minutes and read for 2 seconds on a spectraMAX luminometer. Knockdown was determined by calculating the luciferase signal ratio for each reporter construct for miR-126 over the non-targeting control miRNA. GoClone control reporters used were GAPDH-3'UTR, ACTB-3'UTR, EMPTY-3'UTR, R01, and gene specific reporters were ADAM9-UTR, ILK-UTR, GOLPH3-3'UTR, CDK3-3'UTR and TOM1-3'UTR.

AML Stromal Chemotherapy Assay

Low passage MS5 stromal cells were seeded into 0.1% gelatin coated 96 well tissue culture plates and cultured for 48 hours in H5100 media (SCF; 100 ng/ml, TPO; 50 ng/ml. IL-7; 20 ng/ml, IL-3; 10 ng/ml, IL-6; 20 ng/ml, FLT3L; 10 ng/ml, G-CSF; 20 ng/ml, GM-CSF; 20 ng/ml) with 1% penicillin/streptomycin. After two days, primary patient AML cells (depleted for human T cells; $1x10^5$/well) were plated onto MS5 stroma and cultured overnight. After 24 hours, cells were treated with vehicle or with Daunorubicin/AraC (1:1 ratio; 50 ng/mL Daunorubicin and 500 ng/mL Ara-C) for 72 hours. Cells were recovered and evaluated for live cell content and immuno-phenotype by flow cytometry. Total RNA was recovered for qPCR detection of miR-126 levels.

Intracellular and Phosphoflow

Cultured 8227 cells were washed twice with 1x PBS and pelleted to eliminate culture medium. After washing, cells were stained for CD34 and CD38 cell surface antigens for 20 minutes at RT. Cells were washed and pelleted. Cells were immediately fixed with paraformaldehyde (final

concentration: 1.6%) for 10 minutes at room temperature. Cells were then centrifuged, washed once with PBS 1% BSA to remove residual PFA and permeabilized with ice-cold Perm buffer III (BD Phosflow for 30 min at 4°C followed by 2 washes in order to remove traces of methanol). Intracellular antibody staining was then performed. Phospho-Rb Ser807/811 was detected by a monoclonal antibody (clone D20B12; Cell Signaling), CDK3 was detected by a polyclonal antibody (clone D01P; Abnova) and detected by a donkey anti-rabbit brilliant violet 421 conjugated secondary antibody. Staining was performed by incubating permeabilized cells with the phospho-specific antibody for 30 minutes on ice and at dark, diluted in PBS 1% BSA at a final concentration of 1:50. After incubation, cells were washed in PBS 1% BSA and then stained in secondary antibody for 30 minutes at a final concentration of 1:50. Cells were analyzed by multi-parameter flow cytometry.

Western blot analysis

8227 cells were cultured as described and transduced with viral particles at a multiplicity of infection (MOI) of 30 for at least 16 hours. Cells were allowed to expand for 14 days and then flow sorted for mO^+ cells. Total cellular proteins were extracted with RIPA buffer (20 mM Tris-HCl (pH 7.4), 150 mM NaCl, 5 mM EDTA, 1% Triton X-100) supplemented with protease and phosphatase inhibitors: 1 mM PMSF, 10 mM NaF, 1 mM Na_3VO_4, CompleteMini™ and PhosStop ™ (Roche). Samples were resuspended in the lysis solution and incubated at 4°C for 30 minutes. Cell lysates were cleared by centrifugation at 10,000×g for 10 minutes at 4°C, and the supernatants were collected and assayed for protein concentration using Lowry assay based method (DC, BioRad). 40-50 micrograms of proteins were run on SDS-PAGE under reducing conditions. For immunoblotting, proteins were transferred to PVDF membranes, incubated with the specific antibody (anti-ADAM9 Cell Signaling #2099 1:1000, and ant-pan AKT Cell

Signaling # 4685 1:500, anti-PIK3R2 Cell Signaling #4257 1:1000, and GAPDH 1:10,000, Sigma) followed by peroxidase-conjugated secondary antibodies. Bands were visualized on Kodak BioMax film.

Lentiviral constructs, cell culture and colony formation

Lentiviral vector platforms for ectopic miRNA expression, stable knockdown and live cell miR-reporting were described previously (Gentner et al., 2010). Third generation lentiviral vector particles pseudotyped with VSV-G were generated as described (Guenechea et al., 2000).

8227 cell cultures were initiated from a primary patient sample with outgrowth after 1 month; this stock was used for all experiments. Primitive $CD34^+CD38^-$ 8227 cells were flow sorted and plated in culture media (described in Supplementary Experimental Procedures) for viral transduction and initiation of a new culture that re-establishes the cellular hierarchy. One to two weeks post viral transduction, cultures were re-sorted for $CD34^+CD38^-$ (LSC enriched), $CD34^+CD38^+$ (leukemia progenitor enriched) and $CD34^-CD38^+$ (mature AML blasts) populations for experimental culture studies or colony assays. Individual cultures were passaged weekly and monitored with phenotypic cell surface markers.

For chemotherapy experiments, $1x10^5$ transduced 8227 cells were plated into 96-well plates, exposed the following day to a dose range of Daunorubincin and analyzed using CD34 and CD38 cell surface markers 72 hours later. $CD34^+$ levels were normalized to vehicle only wells.

Ki67 and Hoechst flow cytometry

Cells were stained for surface markers, washed and fixed using BD Cytofix buffer, washed and permeabilized with BD Perm 2 (BD), washed and stained with PE- or FITC- or PerCP-Cy5.5

conjugated Ki67 antibody (BD) and finally resuspended in BD Cytofix buffer with Hoechst at 1 μg/mL. The cells were then analyzed on a BD LSRII machine with a UV laser.

Quantitative PCR

miR-126 expression was analyzed as described (Lechman et al., 2012). Briefly, small RNAs were extracted using Trizol (Life Technologies) and miRNA expression levels were determined by the Applied Biosystems Taqman® microRNA Assay system. Reactions were carried out in triplicate in an ABI Prism 7900HT (Applied Biosystems, Foster City, CA). miRNA expression was normalized to RNU48.

Statistical analysis

Unless otherwise indicated, mean $\pm$ SEM values are reported in the graphs. For pairwise comparisons, a Mann-Whitney non-parametric test was used unless otherwise indicated.

SUPPLEMENTAL REFERENCES

Borgan, Ø. (2001). Modeling Survival Data: Extending the Cox Model. Terry M. Therneau and Patricia M. Grambsch, Springer-Verlag, New York, 2000. No. of pages: xiii + 350. Price: $69.95. ISBN 0-387-98784-3. Stat. Med. *20*, 2053–2054.

Cheson, B.D., Bennett, J.M., Kopecky, K.J., Büchner, T., Willman, C.L., Estey, E.H., Schiffer, C.A., Doehner, H., Tallman, M.S., Lister, T.A., et al. (2003). Revised recommendations of the International Working Group for Diagnosis, Standardization of Response Criteria, Treatment Outcomes, and Reporting Standards for Therapeutic Trials in Acute Myeloid Leukemia. J. Clin. Oncol. Off. J. Am. Soc. Clin. Oncol. *21*, 4642–4649.

Cox, J., and Mann, M. (2008). MaxQuant enables high peptide identification rates, individualized p.p.b.-range mass accuracies and proteome-wide protein quantification. Nat. Biotechnol. *26*, 1367–1372.

Fei, D.L., Koestler, D.C., Li, Z., Giambelli, C., Sanchez-Mejias, A., Gosse, J.A., Marsit, C.J., Karagas, M.R., and Robbins, D.J. (2013). Association between In Utero arsenic exposure, placental gene expression, and infant birth weight: a US birth cohort study. Environ. Health Glob. Access Sci. Source *12*, 58.

Geiss, G.K., Bumgarner, R.E., Birditt, B., Dahl, T., Dowidar, N., Dunaway, D.L., Fell, H.P., Ferree, S., George, R.D., Grogan, T., et al. (2008). Direct multiplexed measurement of gene expression with color-coded probe pairs. Nat. Biotechnol. *26*, 317–325.

Guenechea, G., Gan, O.I., Inamitsu, T., Dorrell, C., Pereira, D.S., Kelly, M., Naldini, L., and Dick, J.E. (2000). Transduction of human CD34+ CD38- bone marrow and cord blood-derived SCID-repopulating cells with third-generation lentiviral vectors. Mol. Ther. J. Am. Soc. Gene Ther. *1*, 566–573.

Hermjakob, H., and Apweiler, R. (2006). The Proteomics Identifications Database (PRIDE) and the ProteomExchange Consortium: making proteomics data accessible. Expert Rev. Proteomics *3*, 1–3.

Hu, Y., and Smyth, G.K. (2009). ELDA: extreme limiting dilution analysis for comparing depleted and enriched populations in stem cell and other assays. J. Immunol. Methods *347*, 70–78.

Johnson, W.E., Li, C., and Rabinovic, A. (2007). Adjusting batch effects in microarray expression data using empirical Bayes methods. Biostat. Oxf. Engl. *8*, 118–127.

Kulak, N.A., Pichler, G., Paron, I., Nagaraj, N., and Mann, M. (2014). Minimal, encapsulated proteomic-sample processing applied to copy-number estimation in eukaryotic cells. Nat. Methods *11*, 319–324.

Lu, J., Getz, G., Miska, E.A., Alvarez-Saavedra, E., Lamb, J., Peck, D., Sweet-Cordero, A., Ebert, B.L., Mak, R.H., Ferrando, A.A., et al. (2005). MicroRNA expression profiles classify human cancers. Nature *435*, 834–838.

Merico, D., Isserlin, R., Stueker, O., Emili, A., and Bader, G.D. (2010). Enrichment map: a network-based method for gene-set enrichment visualization and interpretation. PloS One *5*, e13984.

Reimand, J., Arak, T., and Vilo, J. (2011). g:Profiler--a web server for functional interpretation of gene lists (2011 update). Nucleic Acids Res. *39*, W307–W315.

Rudy, J., and Valafar, F. (2011). Empirical comparison of cross-platform normalization methods for gene expression data. BMC Bioinformatics *12*, 467.

Sirinukunwattana, K., Savage, R.S., Bari, M.F., Snead, D.R.J., and Rajpoot, N.M. (2013). Bayesian hierarchical clustering for studying cancer gene expression data with unknown statistics. PloS One *8*, e75748.

Smoot, M.E., Ono, K., Ruscheinski, J., Wang, P.-L., and Ideker, T. (2011). Cytoscape 2.8: new features for data integration and network visualization. Bioinforma. Oxf. Engl. *27*, 431–432.

Subramanian, A., Tamayo, P., Mootha, V.K., Mukherjee, S., Ebert, B.L., Gillette, M.A., Paulovich, A., Pomeroy, S.L., Golub, T.R., Lander, E.S., et al. (2005). Gene set enrichment analysis: a knowledge-based approach for interpreting genome-wide expression profiles. Proc. Natl. Acad. Sci. U. S. A. *102*, 15545–15550.